RESEARCH ARTICLE

The **FASEB** Journal

Pyruvate kinase modulates the link between β-cell fructose metabolism and insulin secretion

Naoya Murao[1,2] | **Risa Morikawa**[1] | **Yusuke Seino**[1,2] | **Kenju Shimomura**[3] | **Yuko Maejima**[3] | **Tamio Ohno**[4] | **Norihide Yokoi**[5] | **Yuichiro Yamada**[1,2] | **Atsushi Suzuki**[1]

[1]Department of Endocrinology, Diabetes and Metabolism, Fujita Health University, School of Medicine, Toyoake, Japan

[2]Yutaka Seino Distinguished Center for Diabetes Research, Kansai Electric Power Medical Research Institute, Kyoto, Japan

[3]Department of Bioregulation and Pharmacological Medicine, Fukushima Medical University School of Medicine, Fukushima, Japan

[4]Graduate School of Medicine Center for Research of Laboratory Animals and Medical Research Engineering Division for Research of Laboratory Animals, Graduate School of Medicine, Nagoya University, Nagoya, Japan

[5]Laboratory of Animal Breeding and Genetics, Graduate School of Agriculture, Kyoto University, Kyoto, Japan

Correspondence
Naoya Murao, Departments of Endocrinology, Diabetes and Metabolism, Fujita Health University, School of Medicine, 1-98 Dengakugakubo, Toyoake 4701192, Aichi, Japan.
Email: naoya.murao@fujita-hu.ac.jp

Abstract

The intricate link between glucose metabolism, ATP production, and glucose-stimulated insulin secretion (GIIS) in pancreatic β-cells has been well established. However, the effects of other digestible monosaccharides on this mechanism remain unclear. This study examined the interaction between intracellular fructose metabolism and GIIS using MIN6-K8 β-cell lines and mouse pancreatic islets. Fructose at millimolar concentrations potentiated insulin secretion in the presence of stimulatory levels (8.8 mM) of glucose. This potentiation was dependent on sweet taste receptor-activated phospholipase Cβ2 (PLCβ2) signaling. Concurrently, metabolic tracing using ^{13}C-labeled fructose and glucose in conjunction with biochemical analyses demonstrated that fructose blunted the glucose-induced increase in the ATP/ADP ratio. Mechanistically, fructose is substantially converted to fructose 1-phosphate (F1P) at the expense of ATP. F1P directly inhibited PKM2 (pyruvate kinase M2), thereby reducing the later glycolytic flux used for ATP production. Remarkably, F1P-mediated PKM2 inhibition was counteracted by TEPP-46, a small-molecule PKM2 activator. TEPP-46 restored glycolytic flux and the ATP/ADP ratio, leading to the enhancement of fructose-potentiated GIIS in MIN6-K8 cells, normal mouse islets, and

---

Abbreviations: 2PG, 2-phosphoglycerate; 3PG, 3-phosphoglycerate; DHAP, dihydroxyacetone phosphate; F1P, fructose 1-phosphate; FBP, fructose 1,6-bisphosphate; FSIS, fructose-stimulated insulin secretion; G6P, glucose 6-phosphate; F6P, fructose 6-phosphate; GA3P, glyceraldehyde 3-phosphate; GCK, glucokinase; GCKR, glucokinase regulatory protein; GIIS, glucose-induced insulin secretion; IP1, inositol 1-phosphate; K_{ATP} channel, ATP-sensitive K^+ channel; KHK, ketohexokinase; MASLD, metabolic dysfunction-associated steatotic liver disease; OAA, oxaloacetate; PEP, phosphoenolpyruvate; PK, pyruvate kinase; PLC, phospholipase C; STR, sweet-taste receptor.

fructose-unresponsive diabetic mouse islets. These findings reveal an antagonistic interplay between glucose and fructose metabolism in β-cells, highlighting PKM2 as a crucial regulator and broadening our understanding of the relationship between β-cell fuel metabolism and insulin secretion.

1 | INTRODUCTION

Research has established that dietary monosaccharides, such as glucose, fructose, and mannose modulate insulin secretion from pancreatic β-cells.[1,2] Glucose-induced insulin secretion (GIIS) is crucial for glucose homeostasis, and numerous studies have delineated its molecular mechanisms. It is well established that GIIS is regulated by β-cell glucose metabolism through two signaling pathways: the triggering and amplifying pathways.[3,4] The triggering pathway involves the elevation of intracellular Ca^{2+} ($[Ca^{2+}]i$) through various processes. The primary mechanism involves a series of steps following glucose metabolism: an increase in intracellular ATP levels, closure of ATP-sensitive K^+ (K_{ATP}) channels, membrane depolarization, and opening of voltage-dependent Ca^{2+} channels (VDCCs). The amplifying pathway augments the triggering pathway only when the latter is already active through various glucose-related metabolites, such as adenine nucleotides, citrate, GTP, and glutamate.[5–7]

Fructose is the second most abundant monosaccharide in the diet after glucose.[8] It is widely found in fruits and certain sweeteners, making it a significant source of energy for many people. When co-administered with physiological concentrations of glucose, supraphysiological concentrations of fructose enhance insulin secretion in vitro.[1,2,9,10] However, the underlying mechanisms remain only partially understood.

In various cell types, fructose is known to be transported primarily through GLUT5 (SLC2A5) and is converted to F1P by ketohexokinase (KHK), the first rate-limiting enzyme in fructolysis.[11] F1P is then metabolized to glyceraldehyde 3-phosphate (GA3P) and dihydroxyacetone phosphate (DHAP) to enter the glycolytic/gluconeogenic metabolite pool, part of which is used for ATP production[11] (see also Figure 3). Therefore, it is reasonable to hypothesize that fructose metabolism results in increased ATP production and enhanced glucose-GIIS in β-cells. However, this pathway has not yet been conclusively demonstrated. In the present study, we examined β-cell fructose metabolism and its functional relationship with insulin secretion in vitro using clonal β-cell lines and mouse islets.

Surprisingly, the insulinotropic effect of fructose was found to be the result of fructose-activated sweet-taste receptor (STR)-phospholipase Cβ2 (PLCβ2) signaling, fructose metabolism itself playing a minor role. Indeed, we uncovered an antagonistic relationship between glycolysis and fructose metabolism by comprehensive metabolic analysis: fructose 1-phosphate (F1P) inhibited pyruvate kinase M2 (PKM2) while lowering the ATP/ADP ratio. We demonstrate that this F1P-mediated PKM2 inhibition hampers the insulinotropic effect of fructose and that this effect can be mitigated by pharmacological activation of PKM2.

2 | MATERIALS AND METHODS

2.1 | Animals

C57BL/6JJcl (RRID:IMSR_JCL:JCL:MIN-0003) mice were purchased from CLEA Japan (Tokyo, Japan) and used for experiments at 19–20 weeks of age. NSY.B6-Tyr^+, A^y/Hos mice were a gift from Hoshino Laboratory Animals (Ibaraki, Japan) and were used for experiments at 19–20 weeks of age. Mice were maintained under specific-pathogen-free conditions at $23 \pm 2°C$ and $55 \pm 10\%$ relative humidity with 12-h light–dark cycles (8 am–8 pm), with free access to water and standard chow CE-2 (CLEA Japan, Tokyo, Japan). The health status of the mice was checked regularly. All experiments were performed using male mice because female NSY.B6-Tyr^+, A^y/Hos mice typically do not develop hyperglycemia.[12] Body weight and blood glucose levels were measured at 9 am in the ad lib-fed state. The number of mice analyzed is indicated in the figure legends. All animal experiments were performed with the approval APU22080 by the Institutional Animal Care and Use Committee of Fujita Health University, complying with the Guidelines for Animal Experimentation at Fujita Health University and current Japanese guidelines and regulations for scientific and ethical animal experimentation.[13]

2.2 | Cell lines

MIN6-K8 cells were generated as previously described[14] and were kindly provided by Professor Jun-ichi Miyazaki (Osaka University). The cells were cultured in Dulbecco's

modified Eagle's medium (DMEM) containing 4500 mg/L glucose (Sigma-Aldrich, St. Louis, MO, USA, Cat# D5796) supplemented with 10% fetal bovine serum (FBS) (BioWest, Nuaillé, France, Cat# S1400-500) and 5 ppm 2-mercaptoethanol. The cells were maintained at 37°C with 5% CO_2.

2.3 | Plasmids

GW1-PercevalHR was a gift from Gary Yellen (Addgene plasmid # 49082; http://n2t.net/addgene:49082; RRID:Addgene_49082).[15]

2.4 | ReagentsA

Krebs–Ringer bicarbonate buffer-HEPES (133.4 mM NaCl, 4.7 mM KCl, 1.2 mM KH_2PO_4, 1.2 mM $MgSO_4$, 2.5 mM $CaCl_2$, 5 mM $NaHCO_3$, 10 mM HEPES) supplemented with 0.1% bovine-serum albumin (Sigma-Aldrich, St. Louis, MO, USA, Cat# A6003) and 2.8 mM glucose (2.8G-KRBH) adjusted to pH 7.4 was used in in vitro experiments. Additional glucose (final concentration: 8.8 mM), U73122 (CAS: 112648-68-7, Cat# 70740) and fructose were added to KRBH during the stimulation period. Nifedipine (FUJIFILM Wako Pure Chemical, Osaka, Japan, Cat# 14505781), lactisole (Cayman Chemical, Ann Arbor, MI, USA, CAS: 150436-68-3, Cat# 18657), and TEPP-46 (Selleck Chemicals, Houston, TX, USA, CAS: 1221186-53-3, Cat# S7302) were added during the pre-incubation and stimulation periods. The reagents used for stimulation were stored as a 1000× concentrate in dimethyl sulfoxide (DMSO) (FUJIFILM Wako Pure Chemical, Osaka, Japan, Cat# 041-29351) and diluted with KRBH shortly before the experiment. An equal volume of DMSO was added to the vehicle control.

2.5 | Isolation of pancreatic islets from mice

Digesting solution was formulated by supplementing 0.1 w/v% Collagenase from *Clostridium histolyticum* (Sigma-Aldrich, St. Louis, MO, USA, Cat# C6885) to Hanks' balanced salt solution (136.9 mM NaCl, 5.4 mM KCl, 0.8 mM $MgSO_4$, 0.3 mM Na_2HPO_4, 0.4 mM KH_2PO_4, 4.2 mM $NaHCO_3$, 10 mM HEPES, 1.3 mM $CaCl_2$, 2 mM glucose). The mice were euthanized by isoflurane exposure. The pancreas was digested by 10-min incubation at 37°C following intraductal injection of digesting solution. Islets were hand-picked and separated from exocrine tissues, transferred to 60-mm non-treated plates

(AGC Techno Glass, Shizuoka, Japan, Cat# 1010-060), and cultured overnight in RPMI-1640 (Sigma-Aldrich, St. Louis, MO, USA, Cat# R8758) supplemented with 10% FBS (BioWest, Nuaillé, France, Cat# S1400-500) and 1% penicillin–streptomycin solution (FUJIFILM Wako Pure Chemical, Osaka, Japan, Cat# 168-23191) at 37°C with 5% CO_2 before the experiments.

2.6 | Insulin secretion

Insulin secretion was measured using the static incubation method, as described previously.[16,17]

To measure insulin secretion from cell lines, cells were seeded in 24-well plates at a density of 5×10^5 cells/well and cultured for 48 h. On the day of measurement, the cells were subjected to three successive washes with 2.8G-KRBH, followed by a pre-incubation period of 30 min with 300 μL/well of 2.8G-KRBH. Subsequently, the supernatant was replaced with 300 μL/well of fresh KRBH containing the specified stimulations and incubated for 30 min at 37°C. The reaction was terminated by cooling the plate on ice for 10 min, after which the entire supernatant was collected for the quantification of released insulin using the homogeneous time-resolved fluorescence assay (HTRF) Insulin Ultrasensitive kit (Revvity, Waltham, MA, USA, Cat# 62IN2PEH) in accordance with the manufacturer's instructions. Fluorescence was measured using an Infinite F Nano+ microplate reader (Tecan, Zürich, Switzerland).

To measure insulin secretion from islets, overnight cultured islets were rinsed twice with 2.8G-KRBH, followed by pre-incubation with 2.8G-KRBH for 30 min at 37°C. Size-matched islets were hand-picked and dispensed in a 96-well plate (Corning, Glendale, AZ, USA, Cat# 353072) at 5 islets/well. KRBH (100 μL/well) containing the specified stimulations was added and incubated for 30 min at 37°C. The supernatant was subjected to insulin quantification as described above.

2.7 | Measurement of inositol 1-phosphate (IP1)

To measure IP1 content in cell lines, the cells were seeded in a 96-well plate (Corning, Glendale, AZ, USA, Cat# 353072) at a density of 1.0×10^5 cells/well and cultured for 48 h. On the day of measurement, the cells were subjected to three successive washes with IP1 assay buffer (146 mM NaCl, 4.2 mM KCl, 50 mM LiCl, 1 mM $CaCl_2$, 0.5 mM $MgCl_2$, 10 mM HEPES, 0.1% BSA, pH 7.4) supplemented with 2.8 mM glucose (2.8G-IP1 assay buffer), followed by a pre-incubation period of 30 min with 60 μL/well of 2.8G-IP1 assay buffer. Subsequently, 20 μL/well of IP1 assay

buffer containing the specified stimulations at 4× concentration was added to the cells and incubated for another 30 min at 37°C. The cells were lysed by the addition of 20 μL/well lysis buffer from the HTRF IP-One Gq Detection Kit (Revvity, Waltham, MA, USA, Cat# 62IPAPEB). And 30 μL/well of the lysate was transferred to a 384-well low-volume plate (Cat #3826; Corning, Glendale, AZ, USA) and used for IP1 quantification according to the instructions of the HTRF IP-One Gq Detection Kit.

To measure IP1 content in mouse islets, overnight-cultured islets were rinsed twice with 2.8G-IP1 assay buffer, followed by pre-incubation with 2.8G-IP1 assay buffer for 30 min at 37°C. Size-matched islets were hand-picked and dispensed in a 96-well plate (Corning, Glendale, AZ, USA, Cat# 353072) at 5 islets/well. The islets were pre-incubated for 30 min with 45 μL/well of 2.8G-IP1 assay buffer. Subsequently, 15 μL/well of IP1 assay buffer containing the specified stimulations at 4× concentration was added to the cells and incubated for another 30 min at 37°C. The cells were lysed by the addition of 15 μL/well of lysis buffer supplied in the kit. The lysate (30 μL/well) was subjected to IP1 quantification, as described above.

2.8 | Imaging of intracellular Ca^{2+}

Ca^{2+} imaging was performed as previously described.[16] Briefly, cells were seeded in a 35 mm glass-bottom dish (Matsunami Glass, Osaka, Japan, Cat# D11530H) at a density of 1.28×10^5 cells/dish and cultured for 48 h. Subsequently, the cells were loaded with 1 μM Fluo-4 AM (Dojindo, Kumamoto, Japan, Cat# F312) in 2.8G-KRBH for 20 min at 37°C in room air. Following a brief washing, cells were loaded with 1 mL of fresh 2.8G-KRBH and basal recordings were performed for 300 s (from time −300 to 0). Immediately after the addition of 1 mL KRBH supplemented with stimulations at 2× concentration, recordings were resumed for another 600 s (from time 0 to 600) with a time interval of 2 s.

Time-lapse images were obtained using a Zeiss LSM 980 Airyscan2 inverted confocal laser scanning super-resolution microscope equipped with a Plan Apo 40×, 1.4 Oil DICII objective lens (Carl Zeiss Microscopy, Jena, Germany). The cells were excited at a 488 nm laser with 0.3% output power, and fluorescence emission was measured at 508–579 nm. During observation, the cells were maintained at 37°C using an incubator XLmulti S2 DARK (Pecon, Erbach, Germany).

Images were acquired in the frame mode at a rate of 2 frames per second and with an image size of 212.2×212.2 μm (512×512 pixels). The obtained images were analyzed using the ZEN 3.0 imaging software (Carl Zeiss Microscopy, Jena, Germany, RRID:SCR_021725).

Cells were randomly chosen for analysis for each stimulation, and the number of cells analyzed is indicated in the figure legends. The fluorescence intensity of the entire cell body (F) was monitored and normalized to the average fluorescence intensity between −300 and 0 s (F0).

2.9 | Imaging of intracellular ATP/ADP ratio

The Cells were seeded in a 35 mm glass-bottom dish (Matsunami Glass, Osaka, Japan, Cat# D11530H) at a density of 6.0×10^4 cells/dish and cultured for 48 h. Subsequently, the cells were transfected with 0.1 μg/dish of plasmid construct GW1-PercevalHR using Effectene transfection reagent (Qiagen, Venlo, Netherlands, Cat# 301425) in accordance with the manufacturer's instructions. For the simultaneous transfection of GW1-PercevalHR plasmid and siRNA, the DharmaFECT 2 transfection reagent (Dharmacon, Lafayette, CO, USA, Cat# T-2002-03) was employed as an alternative method. The cells were cultured for another 48 h. On the day of the measurement, after a brief washing, the cells were loaded with 1 mL of fresh 2.8G-KRBH, and basal recordings were performed for 300 s (from time −300 to 0). Immediately after the addition of 1 mL KRBH supplemented with stimulations at 2× concentration, recordings were resumed for another 600 s (from time 0 to 600) with a time interval of 2 s.

The cells were excited at 445 nm and 488 nm lasers with 0.8% and 0.3% output power, respectively, and fluorescence emission was measured at 508–543 nm. The ratio (R) of the fluorescence at 445 nm and 488 nm was calculated and normalized to the average fluorescence intensity between −300 and 0 s (R0). The other microscope configurations were the same as those used for Ca^{2+} imaging (Section 2.8).

2.10 | Knockdown experiments using small interfering RNA (siRNA)

siRNAs targeting *Khk* (Dharmacon, Lafayette, CO, USA, Cat# M-062217-01-0005), *Plcb2* (Dharmacon, Lafayette, CO, USA, Cat# M-040977-01-0005), and non-targeting siRNA (Dharmacon, Lafayette, CO, USA, Cat# D-001206-14-50) were reverse-transfected using the DharmaFECT 2 transfection reagent (Dharmacon, Lafayette, CO, USA, Cat# T-2002-03). Briefly, a complex of siRNA and DharmaFECT 2 was prepared in serum-free DMEM (Sigma-Aldrich, St. Louis, MO, USA, Cat# D5796) at a volume of 100 μL/well according to the manufacturer's instructions. Cells were resuspended in complete culture media at 1.25×10^6 cells/mL. The

cell suspension was then combined with the siRNA/ DharmaFECT 2 complex. The final concentrations of siRNA and DharmaFECT 2 were 40 nM and 0.4%, respectively. For insulin secretion and RT-qPCR experiments, the cells were seeded in 24-well plates (Corning, Glendale, AZ, USA, Cat# 353047) at 5×10^5 cells/500 μL/ well. For immunoblotting, the cells were seeded in 12-well plates (Corning, Glendale, AZ, USA, Cat# 353053) at 1×10^6 cells/mL/well. For metabolic flux analysis, cells were seeded in six-well plates (Cat #353046; Corning, Glendale, AZ, USA) at a density of 2×10^6 cells/2 mL/ well. The subsequent experiments were performed after a 48-h culture.

2.11 | Reverse transcription quantitative polymerase chain reaction (RT-qPCR)

cDNA was prepared using CellAmp Direct Lysis and RT set (Takara Bio, Shiga, Japan, Cat# 3737S/A) according to the manufacturer's instructions. Quantitative real-time PCR was performed on a QuantStudio 7 Flex system (Thermo Fisher Scientific, Waltham, MA, USA, RRID:SCR_020245) using TaqMan Universal Master Mix II with UNG (Thermo Fisher Scientific, Waltham, MA, USA, Cat# 4440038) and Taqman probes: *Khk* (Cat# Mm00434647_m1) and TATA-box binding protein (*Tbp*, Cat# Mm01277042_m1). Relative gene expression of *Khk* was calculated using the $2^{-\Delta\Delta CT}$ method and normalized to *Tbp*.

2.12 | Immunoblotting

The cells were lysed with 50 μL/well of RIPA buffer (50 mM Tris–HCl pH 7.4, 150 mM NaCl, 1% NP-40, 0.25% sodium deoxycholate, 1% SDS), and 1x complete protease inhibitor cocktail (Sigma-Aldrich, St. Louis, MO, USA, Cat# 11697498001). The lysate was sonicated for 20 s on ice and centrifuged at $15\,000 \times g$ at 4°C for 10 min. The supernatant was collected and separated on a 7.5% polyacrylamide–SDS gel and transferred to a PVDF membrane. The membranes were blocked with 3% bovine serum albumin (BSA) (Sigma-Aldrich, St. Louis, MO, USA, Cat# A7906) in Tris-buffered saline with Tween 20 (TBS-T) and incubated with anti-KHK mouse monoclonal antibody (1:100) (Santa Cruz Biotechnology, Dallas, TX, USA, Cat# sc-377411) in TBS-T supplemented with 3% BSA overnight at 4°C. The membrane was then incubated with HRP-conjugated anti-mouse immunoglobulins (1:2000) (Agilent, Santa Clara, CA, USA, Cat# P0447, RRID:AB_2617137) in TBS-T supplemented with 1% BSA for 1 h at room temperature. Signals were visualized using ECL Prime

detection reagent (Cytiva, Buckinghamshire, UK, Cat# RPN2232). Images were taken using ImageQuant 800 (Cytiva, Buckinghamshire, UK). Subsequently, the membrane was stripped using Restore Western Blot Stripping Buffer (Thermo Fisher Scientific, Waltham, MA, USA, Cat# 21059) for 15 min and re-probed with an anti-α-tubulin mouse monoclonal antibody (1:1000) (Thermo Fisher Scientific, Waltham, MA, USA, Cat# A11126, RRID:AB_2534135). The images were quantified using ImageJ (version 1.53 k, https://imagej.nih. gov/ij/index.html, RRID:SCR_003070).

2.13 | Metabolic flux analysis

The cells were seeded in six-well plates (Cat #353046; Corning, Glendale, AZ, USA) at 2×10^6 cells/2 mL/well and cultured for 48 h. The cells were then rinsed three times with 2.8G-KRBH, followed by pre-incubation with 2.8G-KRBH for 60 min at 37°C. The supernatant was replaced with KRBH supplemented with specified stimulations including [U-^{13}C]-glucose (Sigma-Aldrich, St. Louis, MO, USA, CAS: 110187-42-3 Cat# 660663) and [U-^{13}C]-fructose (Cambridge Isotope Laboratories, Tewksbury, MA, USA, CAS: 287100-63-4, Cat# CLM-1553-1). The cells were incubated for 30 min at 37°C, and the supernatant was discarded. Cells were quickly rinsed with ice-cold water, extracted by the addition of 500 μL ice-cold extraction buffer (67.5% methanol, 7.5% chloroform, and 25% water), and the whole plate was snap-frozen in liquid nitrogen. Cells were thawed on ice, scraped into 2 mL screw tubes along with the supernatant, and stored at −80°C until extraction of the metabolites.

For extraction of the metabolites, samples were supplemented with 80 μL of diluted (1:640) internal standard (Human Metabolome Technologies, Yamagata, Japan, Cat# H3304-1002), 165 μL of methanol, and 465 μL of chloroform. The samples were then homogenized using a pre-cooled bead crusher at 3200 rpm for 1 min and centrifuged at $15\,000 \times g$ at 4°C for 3 min. The aqueous layer was transferred to pre-wetted ultrafiltration tubes (Human Metabolome Technologies, Yamagata, Japan, Cat# UFC3LCCNB-HMT) and centrifuged at $9100 \times g$, 4°C until completely filtrated. The filtrate was freeze-dried, re-dissolved in 10 μL of water, and subjected to mass spectrometry. The organic layer was evaporated by decompression at room temperature, and the residue was resuspended in RIPA buffer (see Section 2.12) and subjected to a BCA protein assay (Thermo Fisher Scientific, Waltham, MA, USA, Cat# 23225).

cGMP was measured by G7100A capillary electrophoresis (Agilent Technologies, Santa Clara, CA, USA) interfaced with a G6224A time-of-flight LC/MS mass
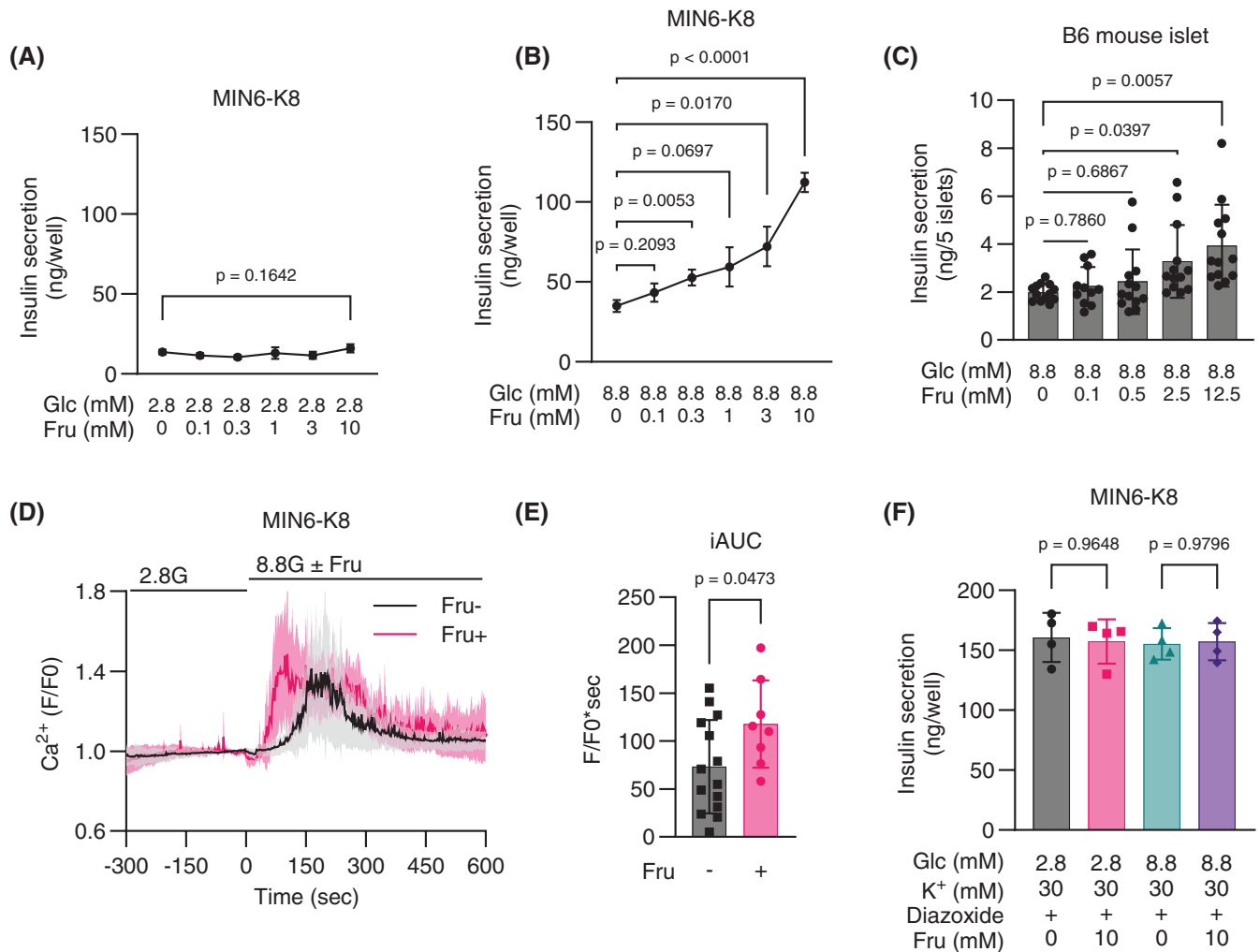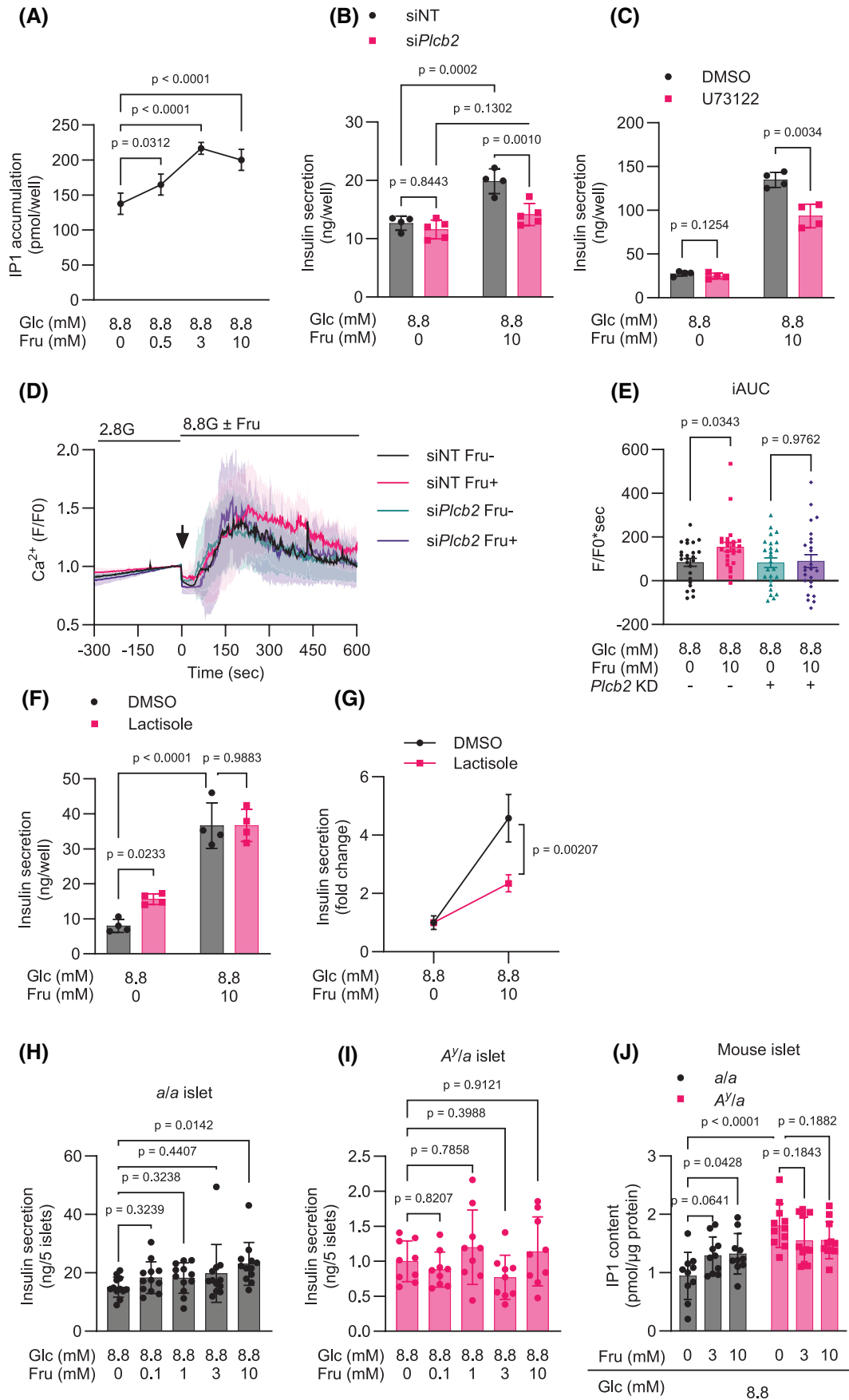
FIGURE 1 Fructose potentiates Ca^{2+} influx and GIIS. (A) Effect of fructose on insulin secretion at 2.8 mM glucose. $n=4$, $N=2$. (B) Dose-dependent effect of fructose on insulin secretion at 8.8 mM glucose. $n=4$, $N=2$. (C) Dose-dependent effect of fructose on insulin secretion at 8.8 mM glucose in B6 mouse islets. Islets were pooled from two mice. $n=11–13$, $N=2$. (D and E) Effect of fructose on intracellular Ca^{2+} levels measured using Fluo-4. The time course of normalized fluorescence intensity at 508–579 nm is indicated in (D). 2.8G, 2.8 mM glucose; 8.8G, 8.8 mM glucose. The magnitude of Ca^{2+} responses was quantified as iAUC in (E), using F/F0 = 1 as the baseline. 8.8 mM Glc: $n=14$; 8.8 mM Glc + 10 mM Fru: $n=8$. $N=2$. (F) Effect of fructose on insulin secretion in the presence of high K^+ and diazoxide (100 μM). $n=4$, $N=2$. All experiments were conducted using MIN6-K8 cells, except for (C). Data are presented as the mean ± standard deviation (SD). Glc, glucose; Fru, fructose. Statistical comparisons were made using Welch's one-way ANOVA with Dunnett's post hoc test for (A–C, and F), and Welch's unpaired two-tailed t-test for (E).

FIGURE 2 Involvement of PLCβ2 signaling in fructose-induced potentiation of GIIS. (A) Dose-dependent effects of fructose on intracellular IP1 accumulation. $n=6$, $N=2$. (B) Effect of *Plcb2* knockdown on fructose-induced potentiation of GIIS. $n=4–5$. $N=2$. (C) Effect of U73122 (20 μM) on fructose-induced potentiation of GIIS. $n=4$. $N=2$. (D and E) Effect of *Plcb2* knockdown on fructose-induced Ca^{2+} increase measured using Fluo-4. siNT 2.8G, 2.8 mM glucose; 8.8G, 8.8 mM glucose. (E) The magnitude of the responses was quantified as iAUC using F/F0 = 1 as the baseline. $n=25$ for each condition. $N=2$. (F and G) Effect of lactisole (50 mM) on fructose-induced potentiation of GIIS. $n=4$. $N=2$. The results are indicated in their original values in (F) and as fold change over 0 mM fructose in (G). $n=4$. $N=2$. (H and I) Fructose-induced potentiation of GIIS in islets of NSY.B6 strains. (H) a/a, $n=9$, $N=2$. (I) A^y/a, $n=12$. $N=2$. Islets were pooled from two mice per strain. (J) Fructose-induced increase in IP1 levels in islets of NSY.B6 strains. The results were normalized to the total protein content. Islets were pooled from two mice per strain. a/a: $n=10$; A^y/a: $n=11$. $N=2$. All experiments were conducted using MIN6-K8 cells, except for (H and I). Glc, glucose; Fru, fructose. Data are presented as the mean ± SD. Statistical comparisons were performed using Welch's one-way ANOVA with Dunnett's post hoc test for (A, E, H, and I), Welch's unpaired two-tailed t-test for (C and G), and two-way ANOVA with Dunnett's post-hoc test for (B, F, and J).
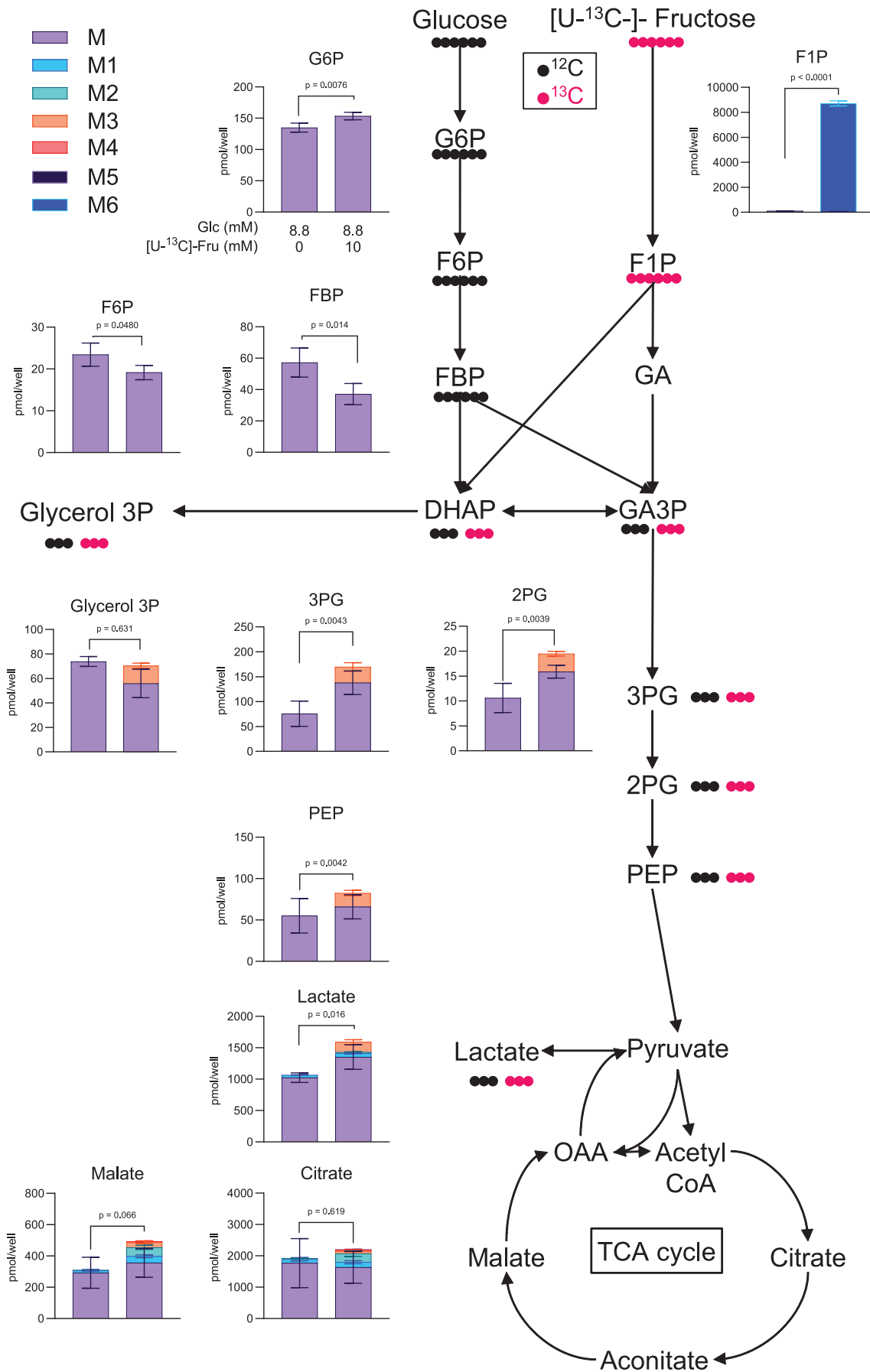
(A)

IP1 accumulation (pmol/well)

p < 0.0001
p < 0.0001
p = 0.0312

Glc (mM) 8.8 8.8 8.8 8.8
Fru (mM) 0 0.5 3 10

(B)
● siNT
■ si*Plcb2*

Insulin secretion (ng/well)

p = 0.0002
p = 0.1302
p = 0.0010
p = 0.8443

Glc (mM) 8.8 8.8
Fru (mM) 0 10

(C)
● DMSO
■ U73122

Insulin secretion (ng/well)

p = 0.0034
p = 0.1254

Glc (mM) 8.8 8.8
Fru (mM) 0 10

(D)

2.8G   8.8G ± Fru

Ca^{2+} (F/F0)

—— siNT Fru−
—— siNT Fru+
—— si*Plcb2* Fru−
—— si*Plcb2* Fru+

Time (sec)

(E) iAUC

F/F0*sec

p = 0.0343
p = 0.9762

Glc (mM) 8.8 8.8 8.8 8.8
Fru (mM) 0 10 0 10
Plcb2 KD − − + +

(F)
● DMSO
■ Lactisole

Insulin secretion (ng/well)

p < 0.0001   p = 0.9883
p = 0.0233

Glc (mM) 8.8 8.8
Fru (mM) 0 10

(G)
—●— DMSO
—■— Lactisole

Insulin secretion (fold change)

p = 0.00207

Glc (mM) 8.8 8.8
Fru (mM) 0 10

(H) *a/a* islet

Insulin secretion (ng/5 islets)

p = 0.0142
p = 0.4407
p = 0.3238
p = 0.3239

Glc (mM) 8.8 8.8 8.8 8.8 8.8
Fru (mM) 0 0.1 1 3 10

(I) *A^y/a* islet

Insulin secretion (ng/5 islets)

p = 0.9121
p = 0.3988
p = 0.7858
p = 0.8207

Glc (mM) 8.8 8.8 8.8 8.8 8.8
Fru (mM) 0 0.1 1 3 10

(J) Mouse islet
● *a/a*
■ *A^y/a*

IP1 content (pmol/μg protein)

p < 0.0001   p = 0.1882
p = 0.0428   p = 0.1843
p = 0.0641

Fru (mM) 0 3 10 0 3 10
Glc (mM) 8.8

spectrometer (Agilent Technologies, Santa Clara, CA, USA). A G1310A isocratic pump (Agilent Technologies, Santa Clara, CA, USA) equipped with a G1379B degasser (Agilent Technologies, Santa Clara, CA, USA) was used to supply sheath liquid (Human Metabolome Technologies, Yamagata, Japan, Cat# H3301-2020). The mass spectrometer was operated in the negative ionization mode. All separations were performed on fused silica capillaries (Human Metabolome Technologies, Yamagata, Japan, Cat# H3305-2002) at 25°C using an anion analysis buffer (Human Metabolome Technologies, Yamagata, Japan, Cat# H3302-2021) as the background electrolyte. The applied voltage was set to 30 kV at 20°C, together with a pressure of 15 mbar. Sheath liquid was delivered to a nebulizer by an isocratic pump at 1 mL/min. Chromatograms and mass spectra were analyzed by MassHunter qualitative analysis version 10.0 (Agilent Technologies, Santa Clara, CA, USA, RRID:SCR_015040). Annotation and quantification of chromatogram peaks were carried out using a standard mixture (Human Metabolome Technologies, Yamagata, Japan, Cat# H3302-2021) as a reference.

2.14 | Measurement of pyruvate kinase (PK) activity

The enzymatic activity of PK was measured using the lactate dehydrogenase (LDH)-linked method, as previously described[18] with several modifications. Purified rabbit L-LDH (Oriental Yeast, Tokyo, Japan, Cat# 46782003) was dissolved in 10% glycerol/PBS to a final concentration of 5000 U/mL. The assay buffer was formulated by combining the following solutions: 100 mM aqueous imidazole hydrochloride (56.7 μL/well), 100 mM aqueous ADP (6 μL/well), 13.1 mM aqueous NADH (1.125 μL/well), 56 mM aqueous phosphoenolpyruvate (2.5 or 7.5 μL/well to achieve final concentrations of 1.87 and 5.6 mM, respectively), 1 M aqueous MgCl$_2$ (1.2 μL/well), 2.5 M aqueous KCl (2.25 μL/well), and 5000 U/mL rabbit L-LDH (0.15 μL/well).

Assays were performed using procedures 6.14.1 and 6.14.2, depending on the sample type.

Curve fitting and calculation of half-maximal inhibitory concentrations (IC50) were performed using GraphPad Prism 10 (Graphpad Software, Boston, MA, USA, https://www.graphpad.com; RRID:SCR_002798).

2.14.1 | Activity of purified recombinant human PKM2

Purified recombinant human PKM2 protein (Sigma-Aldrich, St. Louis, MO, USA; Cat# SAE0021-100UG) was initially dissolved in water at a concentration of 100 μg/mL. The PKM2 standard was prepared by diluting the 100 μg/mL PKM2 solution with 50 mM Tris–HCl buffer (pH 8.5) to final concentrations of 10, 8, 6, 4, 2, and 1 μg/mL. D-Fructose 1-phosphate dipotassium salt (F1P) (Santa Cruz Biotechnology, Dallas, TX, USA, Cat# sc-500907) was initially dissolved in 100 mM aqueous imidazole hydrochloride at 1 M and subsequently added to the assay buffer at the indicated concentrations. TEPP-46 was added to the PKM2 standard and pre-incubated at 30°C for 10 min. The assay buffer was dispensed into a 96-well plate (Greiner Bio-One, Kremsmünster, Austria, Cat# 655101) at 67.5 μL/well and incubated at 30°C for 10 min, followed by the addition of 7.5 μL/well of the human PKM2 standards or lysate samples. Absorbance at 340 nm was recorded at 1-min intervals at 30°C using a Revvity VICTOR Nivo Multimode Microplate Reader (Revvity, Waltham, MA, USA, RRID:SCR_025763). The change in absorbance at 340 nm per minute (ΔAbs340) was measured in the linear portion of the curve. A standard curve was generated by plotting the concentrations of the standards against ΔAbs340. The results are expressed as relative activity to 10 μg/mL PKM2.

2.14.2 | PK activity in cell homogenates

MIN6-K8 cells were seeded in six-well plates at a density of 2×10^6 cells/well and cultured for 48 h. On the day of measurement, the cells were subjected to three successive washes with glucose-free (0G) KRBH, followed by a pre-incubation period of 30 min with 300 μL/well 0G-KRBH. Subsequently, the buffer was replaced with 300 μL/well of 0G-KRBH (Figure 6C) or KRBH containing the specified stimulations (Figure 6D). The cells were incubated for 30 min at 37°C, washed with ice-cold PBS, scraped, and homogenized using a PowerMasher II tissue homogenizer (Nippi, Tokyo, Japan, Cat# 893002). The homogenate was then centrifuged at $15\,000 \times g$ at 4°C for 10 min. For the experiment shown in Figure 6C, the supernatant and assay buffer were supplemented with TEPP-46 and F1P, respectively. For the experiment shown in Figure 6D, no further reagent was added to the supernatant or assay buffer.
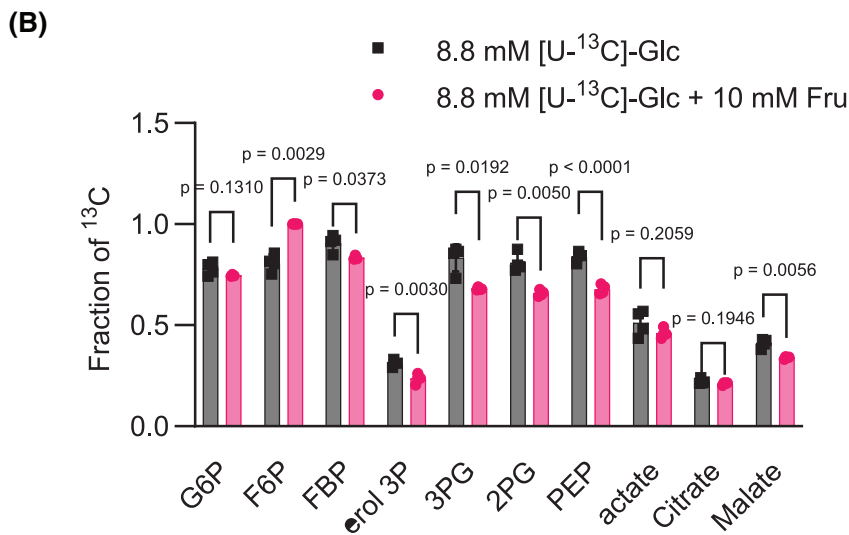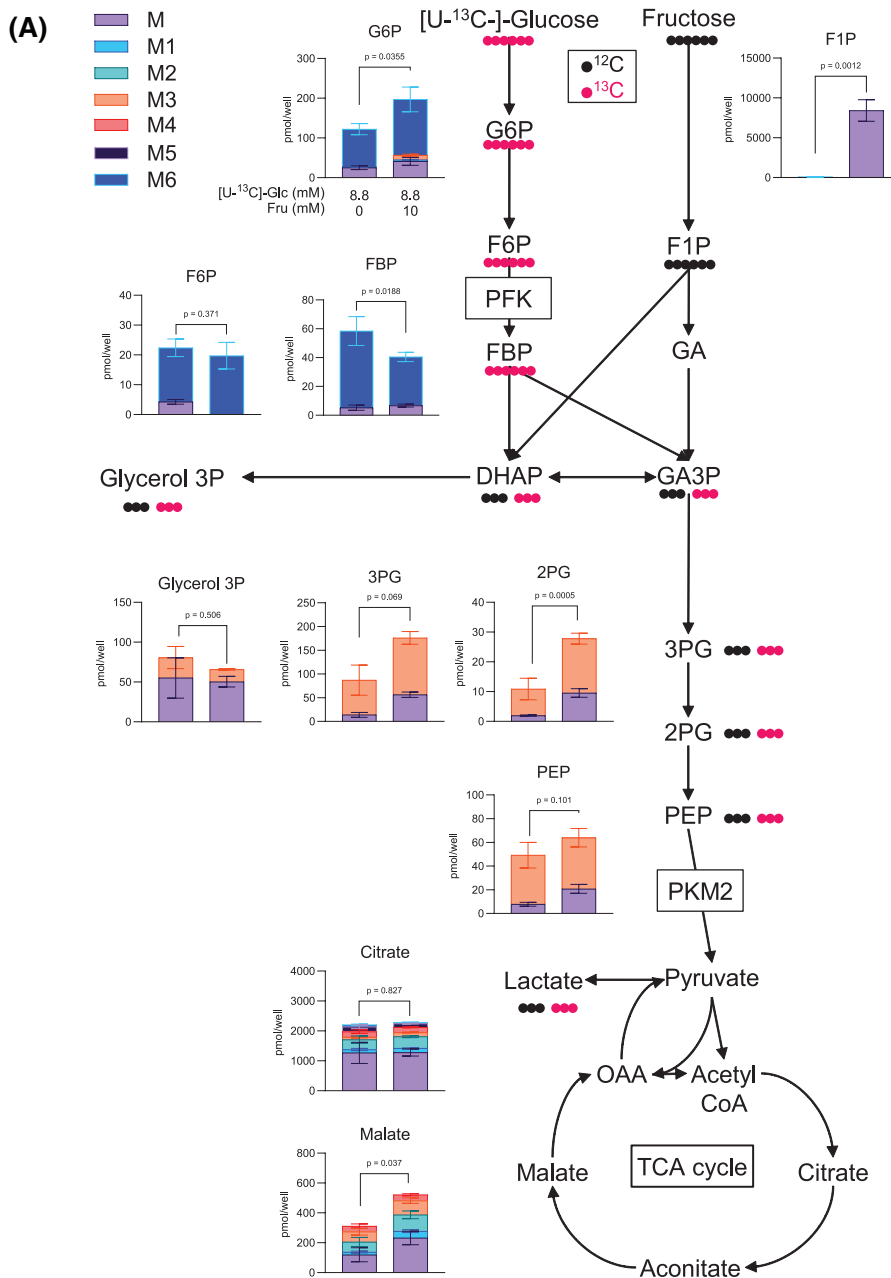
(A)

(B)

FIGURE 4 [U-^{13}C]-glucose tracing in MIN6-K8 cells. (A) The total content and isotopic distribution of each intermediate are indicated as stacked bar graphs alongside a schematic overview of the metabolic fates of [U-^{13}C]-glucose and fructose. $n = 4$, $N = 2$. Statistical comparisons between the sums of all isotopomers were made using Welch's unpaired two-tailed t test. (B) Fraction of ^{13}C in each intermediate. Statistical comparisons were made using Welch's unpaired two-tailed t test. Data are presented as the mean ± standard deviation (SD). Glc, glucose; Fru, fructose.

The measurements and calculations were performed as described in Section 2.14.1. The result was normalized to protein concentrations measured using the BCA Protein Assay (Thermo Fisher Scientific, Waltham, MA, USA, Cat# 23225).

2.15 | Statistical analysis

Sample sizes were estimated from the expected effect size based on previous experiments. No randomization or blinding was used. Experiments were conducted multiple times on separate occasions using distinct cell passages or different mice, with N indicating the number of repetitions. The figures display the representative results from these experiments. For cell line experiments, including insulin secretion, IP1 measurement, RT-qPCR, immunoblotting, and metabolic tracing, n represents the number of biological replicates of cells grown in different wells of the same multi-well plate in a single experiment. For islet experiments, including insulin secretion and IP1 measurement, n represents the number of wells, each containing five islets pooled from multiple age-matched mice. The number of mice used is specified in the figure legends. For Ca^{2+} and ATP/ADP ratio measurements, n represents the number of different single cells analyzed. Data are shown as the mean ± standard deviation (SD) along with the plot of individual data points. For statistical comparisons between two groups, a two-tailed unpaired Welch's unpaired t-test was used. For comparisons between three groups, Welch's one-way analysis of variance (ANOVA) was followed by pairwise comparisons corrected using Dunnett's method. Normality of the distribution was confirmed by the Shapiro–Wilk test. p-values less than .05 were considered statistically significant. The statistical analyses used are indicated in the figure legends. Statistical analyses were performed using GraphPad Prism 10 (Graphpad Software, Boston, MA, USA, https://www.graphpad.com; RRID:SCR_002798).

3 | RESULTS

3.1 | Fructose potentiates GIIS

The dose-dependent effects of fructose on insulin secretion from MIN6-K8 cells and B6 mouse islets were investigated. Fructose had no effect on insulin secretion at basal glucose levels (2.8 mM) in MIN6-K8 cells (Figure 1A). At stimulatory glucose levels (8.8 mM), fructose dose-dependently enhanced insulin secretion at concentrations ranging from 0.3 to 10 mM in MIN6-K8 cells (Figure 1B). A comparable result was observed in B6 mouse islets with 2.5 and 12.5 mM fructose (Figure 1C). These findings indicate that fructose does not independently trigger insulin secretion but potentiates GIIS at millimolar concentrations.

In MIN6-K8 cells at 8.8 mM glucose, fructose enhanced the glucose-induced [Ca^{2+}]i elevation (Figure 1D,E). Additionally, when the membrane potential was clamped in a depolarized state using 30 mM K$^+$ and diazoxide, thereby saturating the triggering pathway, the effect of fructose on GIIS was nullified (Figure 1F). These observations indicate that fructose potentiates GIIS by augmenting the triggering pathway.

3.2 | Fructose-induced potentiation of GIIS requires PLCβ2 signaling

To elucidate the molecular mechanism underlying fructose-enhanced GIIS, we first investigated the potential involvement of sweet taste receptor (STR) signaling. Fructose is known to function as a substrate for STR, a G protein-coupled receptor complex composed of taste receptor type 1 member 2 (TAS1R2) and 3 (TAS1R3).[19–21] STR signals through a second messenger system that involves G-protein gustducin, phospholipase C β2 (PLCβ2), inositol 1,4,5-trisphosphate (IP$_3$), and transient receptor potential M4/5 (TRPM4/5).[22,23] This pathway was originally identified in taste transduction in the tongue.[24] Later studies have shown that STRs are also expressed in β-cells[25] and regulate fructose-induced potentiation of GIIS.[26]

To assess the ability of fructose to activate PLC, d-myo-inositol 1-phosphate (IP1) was quantified as a surrogate for IP$_3$. MIN6-K8 cells exhibited a dose-dependent increase in IP1 when exposed to 0.5 and 3 mM fructose (Figure 2A). The potentiation of GIIS by fructose was eliminated by siRNA-mediated *Plcb2* knockdown (Figure 2B, Figure S1A,B) and partially reduced by U73122, a PLCβ2 inhibitor[27] (Figure 2C). Both *Plcb2* knockdown and U73122 treatment abrogated fructose-induced amplification of glucose-induced [Ca^{2+}]i elevation (Figure 2,

D–E, Figure S1C,D). In addition, we tested the involvement of STRs using lactisole, a TAS1R3 inhibitor that is effective in mice.[28] Lactisole increased insulin secretion at 8.8 mM glucose alone (Figure 2F). This observation aligns with the previously proposed role of STRs in suppressing insulin secretion at moderate glucose concentrations.[29] Notably, this effect was abolished in the presence of fructose (Figure 2F), resulting in a decreased secretory response when expressed as a fold change (Figure 2G). These findings suggest that STR is implicated in fructose-induced potentiation of GIIS.

The association between fructose and PLC signaling was validated in mouse islets. NSY.B6-Tyr^+,A^y is a spontaneous type 2 diabetes mouse strain that was recently established by crossing the NSY and B6J- A^y strains, thereby introducing the obesity-related agouti-yellow (A^y) mutation in the agouti (a) gene into a diabetes-prone NSY background.[12] A^y heterozygous male mouse (A^y/a) displayed obesity and hyperglycemia after 13 weeks of age compared with wild-type male mice (a/a) (Figure S1E,F), as reported previously.[12] Islets were isolated from these mice at 19–20 weeks of age and tested for fructose responsiveness. In a/a mouse islets, 10 mM fructose led to significant increases in GIIS and IP1 levels, but both of these effects were abolished in A^y/a mouse islets (Figure 2H–J). Notably, the elevated baseline IP1 levels in A^y/a islets compared to a/a islets, which indicate enhanced basal PLC activity, may have obscured additional PLC activation by fructose. This basal enhancement may be attributable to chronic hyperglycemia, as we have previously documented.[30] These findings further associate fructose-potentiated GIIS with PLC signaling.

3.3 | Fructose metabolism impedes glycolysis in β-cells

We investigated whether fructose-induced potentiation of GIIS is influenced by intracellular fructose metabolism. According to our previously deposited RNA-seq datasets,[31] $Slc2a5$ (GLUT5) and Khk are expressed in both MIN6-K8 cells and B6 mouse islets (Table S1). To determine whether fructose is metabolized in β-cells, we traced the metabolic fate of ^{13}C-labeled fructose. MIN6-K8 cells were stimulated for 30 min with 10 mM [U-^{13}C]-fructose, a stable isotopomer of fructose in which all six carbon atoms have been replaced with ^{13}C, in the presence of 8.8 mM unlabeled glucose. For each intermediate, ^{13}C-labeled isotopomers were quantified by capillary electrophoresis time-of-flight mass spectrometry (CE-TOFMS) (Figure 3). M–M6 represents the isotopomers in which 0–6 carbon atoms were replaced with [13]C. Naturally occurring

isotopomers are mostly M and M1, whereas incorporation of [U-^{13}C]-fructose-derived carbons generates M2–M6.

Upper glycolytic intermediates, such as G6P, F6P, and FBP, did not comprise M2–M6, whereas F1P was found only as M6 under [U-^{13}C]-fructose treatment. Lower glycolytic intermediates, such as 3PG, 2PG, PEP, glycerol 3P, and lactate, were labeled as M3. Meanwhile, TCA cycle intermediates, such as citrate and malate, were labeled as M2–M6. These results indicate that [U-^{13}C]-fructose enters lower glycolysis and the subsequent TCA cycle. We also assessed labeling efficiency by ^{13}C fraction of the total carbon atoms in each intermediate (Figure S2A). [13]C Fraction was negligible at the basal state and increased up to 0.1–0.2 in the presence of [U-^{13}C]-fructose in glycolysis and TCA cycle intermediates.

Because the insulinotropic effect of fructose was glucose-dependent (Figure 1A,B), we sought to clarify whether fructose affects glucose metabolism. To this end, MIN6-K8 cells were labeled with 10 mM unlabeled fructose in the presence of 8.8 mM [U-^{13}C]-glucose (Figure 4A). Glucose-derived ^{13}C was robustly incorporated into all intermediates, except for F1P. The upper and lower glycolytic intermediates were labeled as M6 and M3, respectively. In those intermediates, the ^{13}C fraction was 0.3–0.5, a value greater than that observed using [U-^{13}C]-fructose at a higher concentration (10 mM), suggesting that the rate of fructose metabolism is lower than that of glucose in β-cells (compare Figure 4B and Figure S2A).

Notably, content (the sum of M–M6) and labeling of several intermediates were significantly affected by fructose. The contents of G6P, 3PG, and 2PG were increased, while that of FBP was decreased by fructose, a trend consistent regardless of the ^{13}C source (Figures 3 and 4A). Additionally, glucose-derived ^{13}C fraction was increased in F6P but was decreased in later steps of glycolysis (Figure 4B). In analyzing these findings, we considered earlier studies that demonstrated the inhibitory effects of high-dose fructose on two key enzymes, phosphofructokinase (PFK)[32] and pyruvate kinase (PK).[33,34] As both PFK and PK reactions are irreversible,[35] it is reasonable to assume that the reduction in their activities causes the accumulation of upstream intermediates and/or the depletion of downstream intermediates. Therefore, increased G6P content, decreased FBP content, and decreased labeling of intermediates after FBP (Figure 4A,B) may reflect reduced PFK activity. In addition, increased contents of 3PG and 2PG are attributable to reduced PK activity. Thus, our ^{13}C tracing experiments revealed an antagonistic interplay between fructose metabolism and glycolysis, demonstrating that while fructose enters lower glycolysis, it simultaneously impedes glycolysis by inhibiting the enzymes PFK and PK.
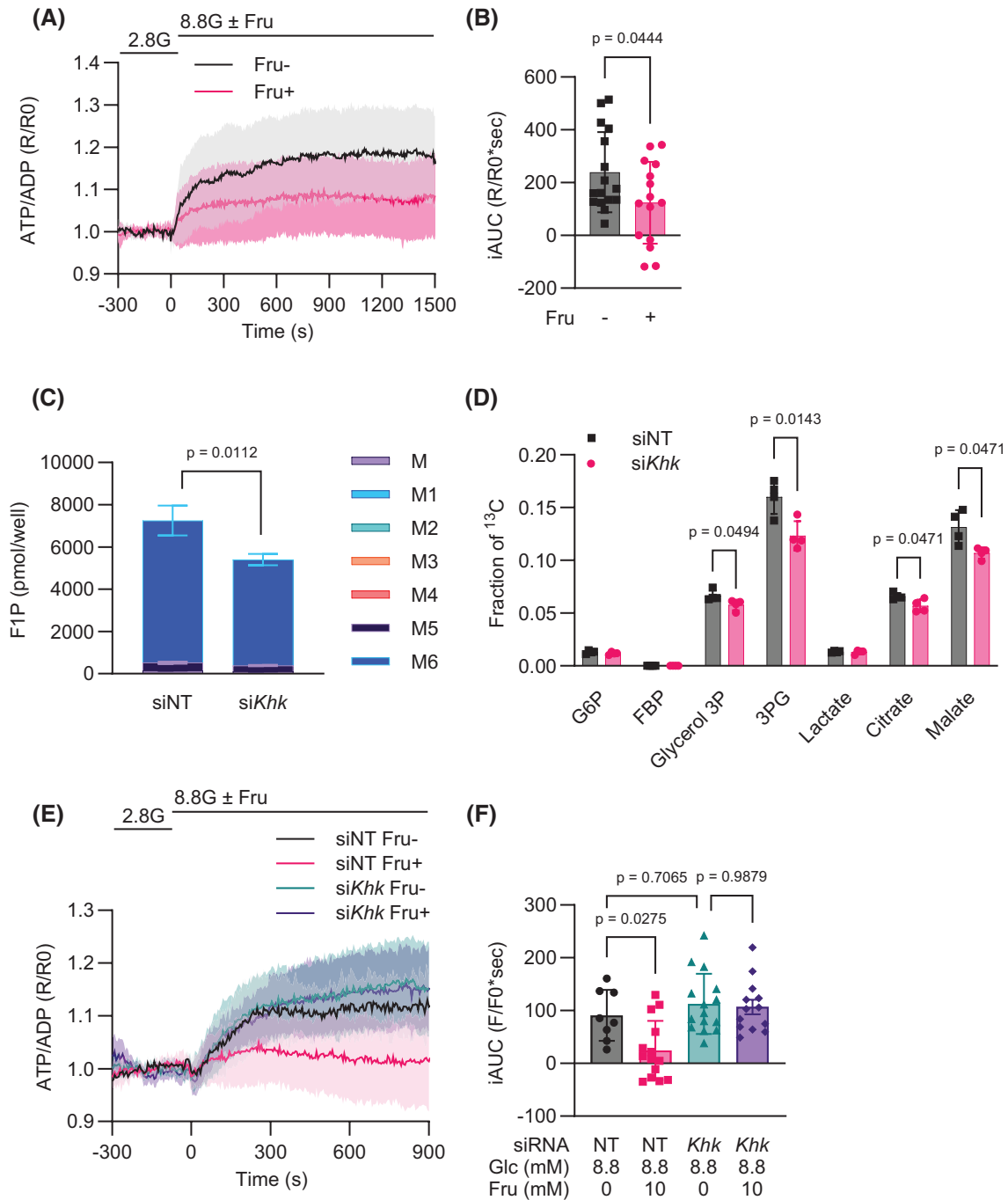
FIGURE 5 Effects of *Khk* knockdown on β-cell energy status. (A and B) Effect of fructose on intracellular ATP/ADP ratio as visualized by Perceval-HR. (A) Time course of normalized ratiometric signals (R/R0). 2.8G, 2.8 mM glucose; 8.8G, 8.8 mM glucose. (B) The magnitude of the responses was quantified as iAUC using R/R0 = 1 as the baseline. Fru−: n = 16, Fru+: n = 15, N = 2. (C and D) [U-13C]-fructose tracing under *Khk* knockdown. The total content and isotopic distribution of F1P are presented in (C). The fraction of 13C in each intermediate is shown in (D). n = 4, N = 2. See Figure S2 for the total content of other metabolites. (E and F) Effect of *Khk* knockdown on intracellular ATP/ADP ratio in MIN6-K8 cells as visualized by Perceval-HR. 2.8G, 2.8 mM glucose; 8.8G, 8.8 mM glucose. (F) The magnitude of the responses was quantified as iAUC using R/R0 = 1 as the baseline. siNT Fru−: n = 8; siNT Fru+: n = 14; si*Khk* Fru−: n = 15; si*Khk* Fru+: n = 13; N = 2. All experiments were performed using MIN6-K8 cells. siNT, non-targeting siRNA; Glc, glucose; Fru, fructose. Data are presented as the mean ± SD. Statistical comparisons were performed using Welch's unpaired two-tailed *t*-test for (B–D), and two-way ANOVA with Dunnett's post hoc test for (F).

3.4 | Fructose suppresses glucose-induced increase in ATP/ADP ratio

We investigated the overall impact of fructose metabolism on the energy status of MIN6-K8 cells. While fructose did not significantly alter the concentrations of adenine nucleotides or redox cofactors (NAD, NADH, NADP, and NADPH), as measured by CE-TOFMS (Figure S2B–D,F–I), we observed a tendency for the ATP/ADP ratio to decrease (Figure S2E). This observation was further supported by time-lapse imaging using PercevalHR, a fluorescent biosensor genetically engineered to measure the ATP/ADP ratio.[15] The imaging revealed that fructose partially reduced the glucose-induced elevation of the ATP/ADP ratio (Figure 5A,B).

To limit fructose metabolism, we employed siRNA to knock down ketohexokinase (*Khk*), which resulted in a decrease of ~70% in mRNA levels and 25% in protein levels (Figure S3A–C). Metabolic phenotypes were examined by [U-^{13}C]-fructose tracing. As expected, *Khk* knockdown decreased M6 F1P (Figure 5C). Although the total content of other intermediates remained unchanged (Figure S4), *Khk* knockdown partially decreased ^{13}C fraction in later glycolysis and TCA intermediates (Figure 5D). Despite the low knockdown efficiency (Figure S3C) resulting in only mild phenotypes, the findings demonstrate that KHK facilitates the flux of fructose into central carbon metabolism. Interestingly, *Khk* knockdown inhibited fructose from reducing the ATP/ADP ratio (Figure 5E,F), suggesting that the reduction in the ATP/ADP ratio is attributable to the KHK reaction (elaborated in Discussion).

3.5 | F1P-induced PKM2 inhibition affects fructose metabolism in β-cells

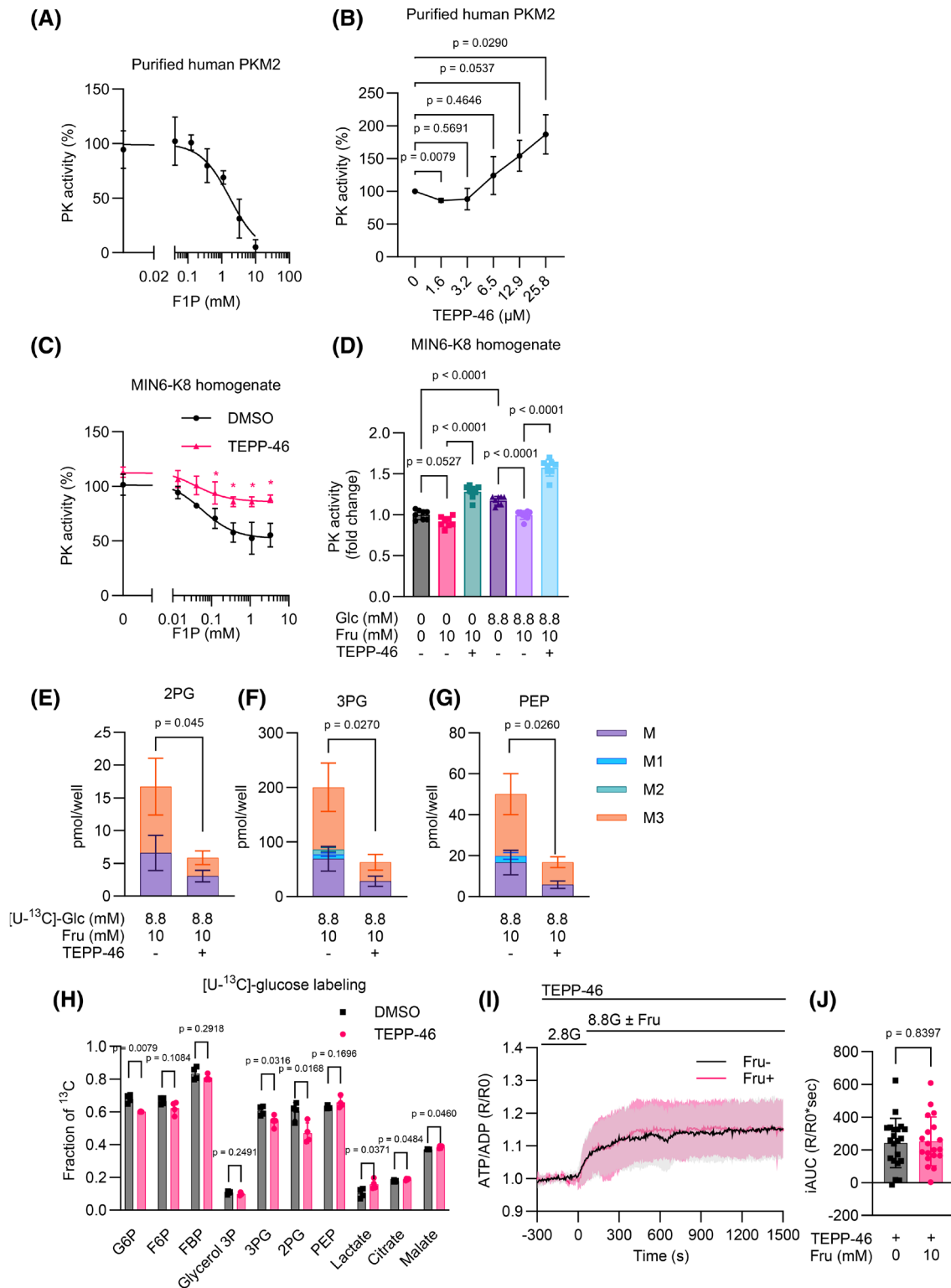One potential explanation for fructose-induced PK inhibition is that F1P binds to and inhibits the M2 isoform of pyruvate kinase (PKM2), as demonstrated in intestinal epithelial cells.[34] Notably, this inhibition can be reversed by TEPP-46, a small-molecule activator of PKM2.[34,36]

Motivated by these findings, we aimed to ascertain whether TEPP-46 enables fructose metabolism to fuel insulin secretion more efficiently. Initially, biochemical assays using recombinant human PKM2 were performed to verify the effects of F1P and TEPP-46. F1P exhibited dose-dependent inhibition of PKM2 (Figure 6A), with an IC50 value of 1.753 (95% confidence interval: 1.223–2.514), which is comparable to the previously reported value.[34] Conversely, TEPP-46 demonstrated dose-dependent activation of PKM2 (Figure 6B). These findings were further corroborated using MIN6-K8 cell homogenate, wherein exogenously applied F1P suppressed PK activity in a dose-dependent manner; however, these effects were counteracted by TEPP-46 (Figure 6C). Similar results were observed when the cells were subjected to glucose, fructose, and TEPP-46 stimulation prior to homogenization (Figure 6D); glucose treatment increased basal PK activity, an effect likely attributable to allosteric activation by FBP.[37] Fructose suppressed PK activity irrespective of the glucose concentration; nevertheless, this suppression was successfully restored by TEPP-46 (Figure 6D).

To assess TEPP-46's in situ effects, we conducted metabolic tracing studies using either [U-^{13}C]-glucose or [U-^{13}C]-fructose with TEPP-46. Both experiments showed that TEPP-46 notably decreased the fructose-induced buildup of 2PG, 3PG, and PEP (Figure 6E–G, Figures S5 and S6A). These observations align with the effects observed when PK is activated in hepatocytes.[38]

In [U-^{13}C]-glucose tracing, ^{13}C fraction in 3PG and 2PG was decreased, while that in later intermediates (lactate, citrate, and malate) was increased (Figure 6H). Similarly, in [U-^{13}C]-fructose tracing, the ^{13}C fraction in citrate and

FIGURE 6 PK activator TEPP-46 counteracts F1P-induced PKM2 inhibition in β-cells. (A–D) Biochemical assay of PK activity. PEP concentration used is 1.87 mM for (A and C), and 5.6 mM for (B and D). Data are expressed as % activity in (A–C) or as fold change over the untreated control in (D). (A) Dose-dependent effects of F1P on the activity of purified recombinant human PKM2. $n = 4$, $N = 2$. (B) Dose-dependent effects of TEPP-46 on the activity of purified recombinant human PKM2. $n = 4$, $N = 2$. (C) Effect of TEPP-46 on F1P-induced inhibition of PK activity in MIN6-K8 cell homogenates. $n = 3$, $N = 2$. (D) PK activity in homogenates of MIN6-K8 cells pretreated with indicated stimulations. Data were normalized to total protein levels. $n = 8$, $N = 2$. (E–H) [U-^{13}C]-Glucose tracing in the presence of TEPP-46. The total content and isotopic distribution of the lower glycolytic intermediates are presented in (E–G). The fraction of ^{13}C in each intermediate is presented in (H). $n = 4$, $N = 2$. See Figure S5 for the total content and isotopic distribution of the other metabolites. (I and J) Effect of fructose on the intracellular ATP/ADP ratio in the presence of TEPP-46 as visualized by Perceval-HR. Fru−: $n = 21$; Fru+: $n = 19$, $N = 2$. (F) Time course of normalized ratiometric signals (R/R0). (G) The magnitude of the responses was quantified as iAUC using R/R0 = 1 as the baseline. 2.8G, 2.8 mM glucose; 8.8G, 8.8 mM glucose. Experiments (C–J) were performed using MIN6-K8 cells. Glc, glucose; Fru, fructose. The following methods were used for statistical analysis: For (B), data from three separate experiments ($n = 1$, $N = 3$) were pooled and evaluated using repeated measures one-way ANOVA followed by Dunnett's post hoc test; For (C), Welch's unpaired two-tailed *t*-test was used; For (D), Welch's one-way ANOVA with Dunnett's post hoc test was used; For (E–G), the sum of all isotopomers was compared using Welch's unpaired two-tailed *t*-test; For (H and J), Welch's unpaired two-tailed *t*-test was used. *$p < .05$.

(A) Purified human PKM2

(B) Purified human PKM2

(C) MIN6-K8 homogenate

(D) MIN6-K8 homogenate

(E) 2PG

(F) 3PG

(G) PEP

(H) [U-^{13}C]-glucose labeling

(I)

(J)

malate slightly, but significantly, increased (Figure S6B). These results suggest that TEPP-46 facilitates the metabolic flux of glucose and fructose after the PK step. In the presence of TEPP-46, fructose did not inhibit glucose-induced elevation of the ATP/ADP ratio (Figure 6I,J). These findings indicate that TEPP-46 counteracted F1P-induced PK inhibition, thereby restoring the ATP/ADP ratio.

3.6 | Mitigating F1P-induced PKM2 inhibition enhances insulin secretion

TEPP-46 demonstrated a notable enhancement of fructose-potentiated GIIS, whereas it exhibited no effect on GIIS alone (Figure 7A). Consistently, TEPP-46 amplified the Ca^{2+} response in the presence of both

glucose and fructose (Figure 7D,E) but did not affect the Ca²⁺ response triggered solely by glucose (Figure 7B,C).

Khk knockdown did not influence glucose-induced insulin secretion (GIIS) or its enhancement by fructose in the absence of TEPP-46. However, it significantly reduced
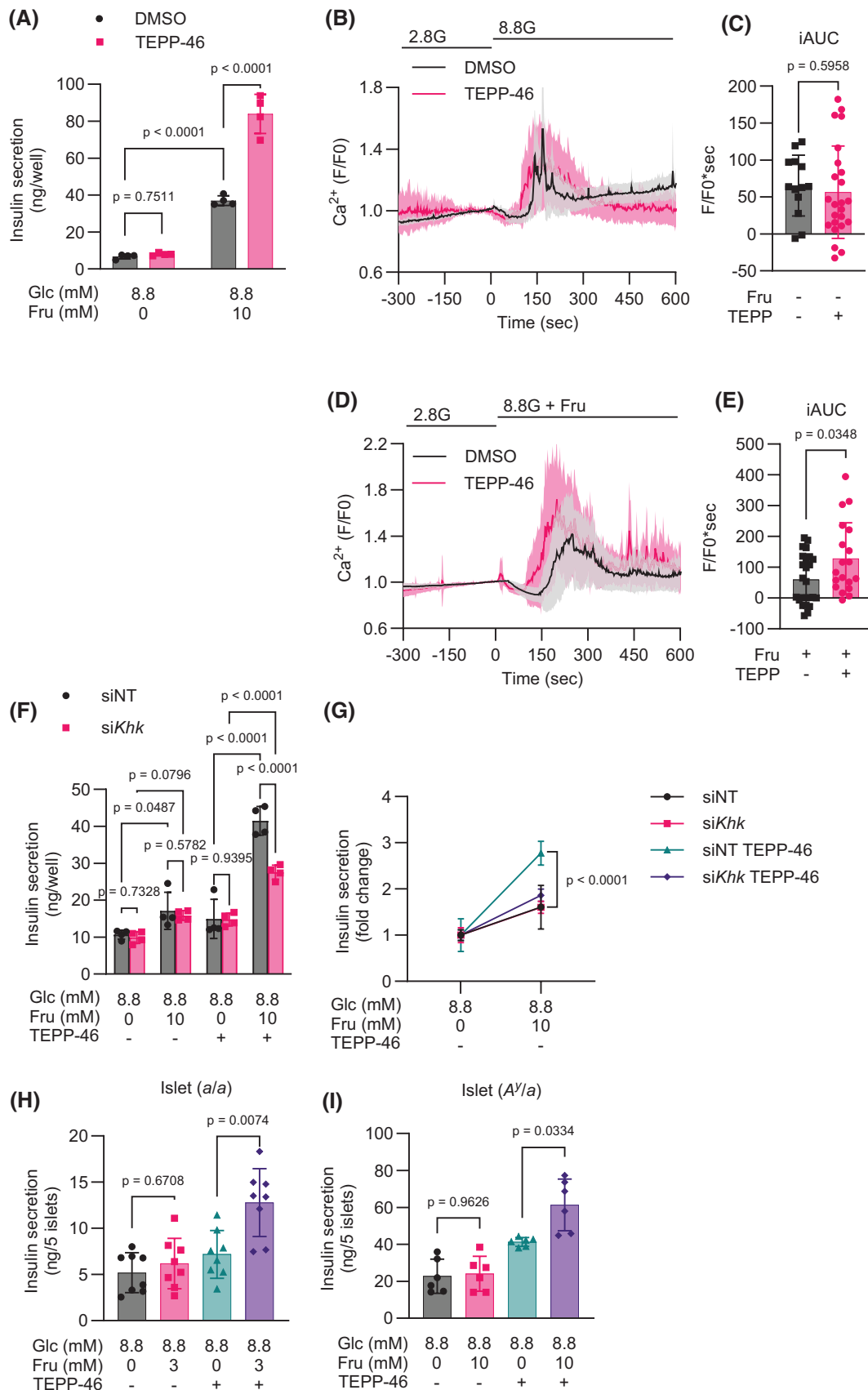
FIGURE 7 PK activator TEPP-46 enhances β-cell fructose responsiveness. (A) Effect of TEPP-46 on fructose-induced potentiation of GIIS. $n=4$, $N=2$. (B–E) Effects of TEPP-46 on glucose-induced Ca^{2+} increase in the absence or presence of fructose. (B) DMSO: $n=13$; TEPP-46: $n=24$, $N=2$. 2.8G, 2.8 mM glucose; 8.8G, 8.8 mM glucose. (C) The magnitude of the responses in (B) was quantified as iAUC using F/F0 = 1 as the baseline. (D) DMSO: $n=25$; TEPP-46: $n=24$, $N=2$. (E) The magnitude of the responses was quantified as iAUC using F/F0 = 1 as the baseline. (F and G) Effect of *Khk* knockdown on fructose-stimulated GIIS in the absence or presence of TEPP-46. siNT, non-targeting siRNA. $n=4$, $N=2$. The data are expressed as the fold change in (G). (H and I) Effects of TEPP-46 on FSIS in islets of NSY. B6 strains. (H) A^y/a mouse islets, $n=8$, $N=2$. (I) a/a mouse islets, $n=6$, $N=2$. Islets were pooled from two mice per strain. Experiments in (A–G) were performed using MIN6-K8 cells. TEPP-46 was used at a concentration of 10 μM. Data are presented as the mean ± SD. Statistical comparisons were performed using two-way ANOVA with Dunnett's post hoc test for (A and F), Welch's unpaired two-tailed *t*-test for (C, E and G), and Welch's one-way ANOVA with Dunnett's post hoc test for (H and I).

TEPP-46-mediated augmentation of fructose-potentiated GIIS (Figure 7F). Under *Khk* knockdown conditions, fructose amplified GIIS to a comparable extent regardless of TEPP-46 presence (Figure 7G), an effect likely mediated by PLCβ2. These findings suggest that fructose metabolism has no impact on insulin secretion in the absence of TEPP-46; however, it effectively fuels insulin release in the presence of TEPP-46.

Finally, we evaluated TEPP-46 in NSY.B6-*Tyr*⁺, A^y strain islets. In *a/a* mouse islets, 3 mM fructose by itself did not enhance GIIS, but exhibited significant enhancement when combined with TEPP-46 (Figure 7H). A comparable outcome was observed in A^y/a islets treated with 10 mM fructose (Figure 7I). These findings support the efficacy of PKM2 activation in improving fructose sensitivity in both healthy and diabetic β-cells.

4 | DISCUSSION

The present study reveals how fructose is "disallowed" as a metabolic fuel for insulin secretion, illuminating PKM2 as a crucial regulator. Our findings demonstrate that: (1) fructose-activated PLCβ2 signaling plays a more crucial role in insulin secretion than fructose metabolism; (2) fructose metabolism inhibits glycolysis and lowers the ATP/ADP ratio through F1P-induced PKM2 inhibition; and (3) a small-molecule PK activator can counteract F1P-induced PKM2 inhibition.

Our results show that fructose-potentiated insulin secretion and fructose metabolism are not directly associated. For example, fructose increased GIIS despite its suppression of the glucose-induced increase in the ATP/ADP ratio (Figure 5A). Moreover, *Khk* knockdown significantly altered fructose metabolic flux and the ATP/ADP ratio (Figure 5D,E) but did not affect fructose-induced potentiation of GIIS (Figure 7F). In contrast, *Plcb2* knockdown abolished the effect of fructose on insulin secretion, demonstrating that PLCβ2 signaling plays a greater role in GIIS than fructose metabolism itself. These findings align well with a previous study demonstrating that fructose enhances insulin secretion through PLCβ2 signaling

and subsequent activation of transient receptor potential cation channel subfamily M, member 5 (TRPM5).[26] TRPM5 has been shown to produce small background inward currents and promote β-cell electrical activity, thereby enhancing Ca^{2+} influx and insulin secretion.[40,41] Importantly, these effects become substantial only when the conductance of β-cell membranes is already reduced owing to K_{ATP} channel closure.[42] This concept also aligns with the finding that the effect of fructose on insulin secretion is muted at low glucose levels (Figure 1A) and after pre-treatment with diazoxide.[43] This also suggests that an increase in the ATP/ADP ratio caused by the combination of fructose and glucose is adequate to close the K_{ATP} channels (Figure 5A).

Researchers have long recognized that β-cells can metabolize fructose.[1,10,44,45] However, the present study offers certain technical advantages over previous experiments. For example, early studies used radioisotope-labeled sugars, which suggested that the utilization and oxidation rates of glucose remained unchanged in the presence of excess fructose at the whole-islet level.[10] In contrast, our ^{13}C metabolic tracing technique enabled quantification of metabolic flux at the substrate level, revealing a reduction in downstream glycolysis in the presence of fructose. These findings indicate that the overall cellular glucose utilization rate is controlled primarily by glucokinase (GCK) activity, potentially masking variations in subsequent metabolic steps.

Fructose in the liver enhances glucose uptake and phosphorylation by dissociating GCK from glucokinase regulatory protein (GCKR).[46,47] However, this process is unlikely to occur in β-cells, considering the extremely low expression levels of *Gckr* (Table S1). Instead, the observed increase in G6P by fructose was likely the result of diminished PFK activity. Contrary to previous studies suggesting that fructose is converted to F6P and G6P,[44,45] we detected no conversion of [U-^{13}C]-fructose into M6 F6P or M6 G6P (Figure 3).

In accordance with previous studies,[10,44,45,48] the rate of fructose metabolism was found to be significantly lower than that of glucose metabolism in β-cells. Previous studies have suggested that fructose enhances GIIS by serving as a substrate for ATP generation. This hypothesis was

based on the observed correlation between insulin secretion rates and fructose metabolism or ATP production.[10,45] However, these findings are challenged by later studies using diabetic GK rats[44] and an INS-1E β-cell line[49] that found no impact of acute fructose on mitochondrial respiration or ATP production, as well as by our observation that fructose impedes the glucose-induced increase in the ATP/ADP ratio.

We note two critical processes in the fructose metabolic pathway that hamper glucose-induced increases in the ATP/ADP ratio: ATP hydrolysis by KHK and F1P-induced inhibition of PKM2. Phosphorylation of fructose by KHK requires ATP hydrolysis, which leads to a reduction in ATP levels in the liver and kidney cells.[39,50,51] In addition, chronic fructose treatment has been shown to decrease ATP levels in INS-1E cells.[49] We found in MIN6-K8 cells that M6 F1P accumulated substantially after [U-^{13}C]-fructose treatment (~40 times more than G6P) while ^{13}C incorporation in downstream intermediates was relatively low, which may be the result of an imbalance between the abundant expression of KHK and the very low expression of aldolase B (Table S1). As *Khk* knockdown prevented a decrease in the ATP/ADP ratio, we surmise that ATP consumption by KHK could not be supplemented by subsequent ATP production via fructose catabolism.

PK has three isoforms: PKM1, PKM2 (both encoded by *Pkm*), and PKLR (encoded by *Pklr*). Our RNA-seq data reveal that *Pkm* is expressed more prominently than *Pklr* in MIN6-K8 cells and B6 mouse islets (Table S1). This aligns with the finding that β-cell PK activity comprises 90% PKM1, 10% PKM2, and no detectable contribution from PKLR.[52] Considering that F1P inhibition and TEPP-46 activation are both specific to PKM2,[34,53] it is likely that PKM1 accounts for the remaining PK activity observed in fructose-treated β-cells during metabolic tracing (Figure 4) and biochemical experiments (Figure 6A).

Research has shown that TEPP-46 enhances GIIS without fructose.[38,52,53] When only glucose is present, TEPP-46 does not boost glucose oxidation or the ATP/ADP ratio, but instead increases the rate of ATP/ADP cycling.[52,53] The impact of TEPP-46 on glucose-induced insulin secretion (GIIS) is dependent on glucose levels; it shows minor effects at moderate glucose concentrations but exhibits a considerably more pronounced effect when glucose levels are high.[38,53] In line with this, TEPP-46 is found not to alter GIIS at moderate glucose concentrations (8.8 mM) (Figure 7A). Nevertheless, in the presence of fructose, TEPP-46 elevated the ATP/ADP ratio, counteracting fructose-induced reduction (Figure 6I) and markedly enhancing GIIS (Figure 7A). These findings indicate that glucose and fructose differentially regulate PK during glycolysis. First, at moderate glucose levels, PK activity is adequate to process the PEP supply, resulting in minimal impact of TEPP-46 on GIIS. Second, when fructose is introduced alongside moderate glucose, F1P reduces PK activity while fructose-derived carbons increase glycolytic load, resulting in PK activity falling short of the elevated PEP supply. In this case, ATP consumption by KHK cannot be compensated for by ATP production after PK. Third, TEPP-46 prevents this inhibition, enabling PKM2 to manage the increased PEP supply for oxidative phosphorylation, leading to an increase in the ATP/ADP ratio.

Recent studies have suggested that ATP supplied directly by membrane-bound PK to K_{ATP} channels regulates their activity.[52–55] Although this theory is debated,[56–58] enhanced ATP/ADP turnover near K_{ATP} channels may contribute to the effect of TEPP-46 on fructose-enhanced GIIS.

To summarize, our investigation uncovers an antagonistic relationship between glucose and fructose metabolism at PKM2 and sheds light on the emerging importance of PK in insulin release, expanding our knowledge of how β-cell fuel metabolism regulates insulin secretion.

5 | LIMITATIONS OF THE STUDY

Our present findings shed light on the unique metabolic properties of fructose, a common dietary sugar, but their physiological relevance should be approached with caution.

There is a large disparity between our experimental and physiological fructose concentrations. However, studies of fructose-potentiated GIIS have consistently employed fructose concentrations in the millimolar range from 3 to 27.5 mM.[2,9,10,26,49] This approach was mirrored in the present study, in which fructose was generally used at 10 mM, a level comparable to that of glucose (8.8 mM). In contrast, physiological blood fructose levels are in the micromolar range, from 1/10 to 1/1000 of blood glucose concentrations.[59–61] At these lower concentrations, fructose failed to enhance GIIS (Figure 1B,C), suggesting that fructose-potentiated GIIS has limited physiological relevance. To illuminate the intricate link between β-cell glycolysis and insulin secretion, we employed supraphysiological fructose concentrations that cause a significant secretory response.

DISCLOSURES

The authors declare no conflict of interest.

DATA AVAILABILITY STATEMENT

The RNA sequencing data used for Table S1 are available from the DDBJ Sequence Read Archive with the accession number DRA006332.[31] Other data supporting the findings of this study are available from the corresponding author upon reasonable request.

ORCID

Naoya Murao https://orcid.org/0000-0002-7424-4476
Risa Morikawa https://orcid.org/0009-0004-1918-2649
Yusuke Seino https://orcid.org/0000-0002-9099-3493
Kenju Shimomura https://orcid.org/0000-0002-1539-2532
Yuko Maejima https://orcid.org/0000-0001-5370-5758
Tamio Ohno https://orcid.org/0009-0005-9248-2880
Norihide Yokoi https://orcid.org/0000-0002-5596-9754
Yuichiro Yamada https://orcid.org/0000-0003-1623-0815
Atsushi Suzuki https://orcid.org/0000-0003-0807-199X

REFERENCES

1. Ashcroft SJ, Bassett JM, Randle PJ. Insulin secretion mechanisms and glucose metabolism in isolated islets. *Diabetes*. 1972;21(Supplement_2):538-545. doi:10.2337/diab.21.2.S538

2. Grodsky GM, Batts AA, Bennett LL, Vcella C, McWilliams NB, Smith DF. Effects of carbohydrates on secretion of insulin from isolated rat pancreas. *Am J Physiol Legacy Content*. 1963;205(4):638-644. doi:10.1152/ajplegacy.1963.205.4.638

3. Henquin J-C. Triggering and amplifying pathways of regulation of insulin secretion by glucose. *Diabetes*. 2000;49:1751-1760.

4. Henquin J-C. Regulation of insulin secretion: a matter of phase control and amplitude modulation. *Diabetologia*. 2009;52:739-751.

5. Han G, Takahashi H, Murao N, et al. Glutamate is an essential mediator in glutamine-amplified insulin secretion. *J Diabetes Investig*. 2021;12:920-930.

6. Murao N, Yokoi N, Honda K, et al. Essential roles of aspartate aminotransferase 1 and vesicular glutamate transporters in β-cell glutamate signaling for incretin-induced insulin secretion. *PLoS One*. 2017;12(11):e0187213. doi:10.1371/journal.pone.0187213

7. Prentki M, Matschinsky FM, Madiraju SM. Metabolic signaling in fuel-induced insulin secretion. *Cell Metab*. 2013;18(2):162-185. doi:10.1016/j.cmet.2013.05.018

8. Larke JA, Bacalzo N, Castillo JJ, et al. Dietary intake of monosaccharides from foods is associated with characteristics of the gut microbiota and gastrointestinal inflammation in healthy US adults. *J Nutr*. 2023;153(1):106-119. doi:10.1016/j.tjnut.2022.12.008

9. Grant A, Christie M, Ashcroft S. Insulin release from human pancreatic islets in vitro. *Diabetologia*. 1980;19(2):114-117. doi:10.1007/BF00421856

10. Zawalich WS, Rognstad R, Pagliara AS, Matschinsky FM. A comparison of the utilization rates and hormone-releasing actions of glucose, mannose, and fructose in isolated pancreatic islets. *J Biol Chem*. 1977;252:8519-8523.

11. Hannou SA, Haslam DE, McKeown NM, Herman MA. Fructose metabolism and metabolic disease. *J Clin Invest*. 2018;128:545-555.

12. Ohno T, Miyasaka Y, Yoshida K, et al. A novel model mouse for type 2 diabetes mellitus with early onset and persistent hyperglycemia. *Exp Anim*. 2022;71:510-518.

13. Kagiyama N, Ikeda T, Nomura T. Japanese guidelines and regulations for scientific and ethical animal experimentation. *In Vivo Models of Inflammation: Volume I*. Springer; 2006:187-191.

14. Iwasaki M, Minami K, Shibasaki T, Miki T, Miyazaki J i, Seino S. Establishment of new clonal pancreatic β-cell lines (MIN6-K) useful for study of incretin/cyclic adenosine monophosphate signaling. *J Diabetes Investig*. 2010;1:137-142.

15. Tantama M, Martínez-François JR, Mongeon R, Yellen G. Imaging energy status in live cells with a fluorescent biosensor of the intracellular ATP-to-ADP ratio. *Nat Commun*. 2013;4:2550.

16. Murao N, Morikawa R, Seino Y, et al. Sildenafil amplifies calcium influx and insulin secretion in pancreatic β cells. *Physiol Rep*. 2024;12(11):e16091. doi:10.14814/phy2.16091

17. Murao N, Yokoi N, Takahashi H, Hayami T, Minami Y, Seino S. Increased glycolysis affects β-cell function and identity in aging and diabetes. *Mol Metab*. 2022;55:101414. doi:10.1016/j.molmet.2021.101414

18. Sakai H, Suzuki K, Imahori K. Purification and properties of pyruvate kinase from Bacillus stearothermophilus. *J Biochem*. 1986;99(4):1157-1167. doi:10.1093/oxfordjournals.jbchem.a135579

19. Chandrashekar J, Hoon MA, Ryba NJ, Zuker CS. The receptors and cells for mammalian taste. *Nature*. 2006;444(7117):288-294. doi:10.1038/nature05401

20. Nelson G, Hoon MA, Chandrashekar J, Zhang Y, Ryba NJ, Zuker CS. Mammalian sweet taste receptors. *Cell*. 2001;106:381-390.

21. Zhao GQ, Zhang Y, Hoon MA, et al. The receptors for mammalian sweet and umami taste. *Cell*. 2003;115(3):255-266. doi:10.1016/s0092-8674(03)00844-4

22. Huang L, Shanker YG, Dubauskaite J, et al. Gγ13 colocalizes with gustducin in taste receptor cells and mediates IP3 responses to bitter denatonium. *Nat Neurosci*. 1999;2:1055-1062.

23. Zhang Z, Zhao Z, Margolskee R, Liman E. The transduction channel TRPM5 is gated by intracellular calcium in taste cells. *J Neurosci*. 2007;27:5777-5786.

24. Ahmad R, Dalziel JE. G protein-coupled receptors in taste physiology and pharmacology. *Front Pharmacol*. 2020;11:587664. doi:10.3389/fphar.2020.587664

25. Nakagawa Y, Nagasawa M, Yamada S, et al. Sweet taste receptor expressed in pancreatic β-cells activates the calcium and cyclic AMP signaling systems and stimulates insulin secretion. *PLoS One*. 2009;4(4):e5106. doi:10.1371/journal.pone.0005106

26. Kyriazis GA, Soundarapandian MM, Tyrberg B. Sweet taste receptor signaling in beta cells mediates fructose-induced potentiation of glucose-stimulated insulin secretion. *Proc Natl Acad Sci USA*. 2012;109(8):E524-E532. doi:10.1073/pnas.1115183109

27. Bleasdale JE, Thakur NR, Gremban RS, et al. Selective inhibition of receptor-coupled phospholipase C-dependent processes in human platelets and polymorphonuclear neutrophils. *J Pharmacol Exp Ther*. 1990;255:756-768.

28. Hamano K, Nakagawa Y, Ohtsu Y, et al. Lactisole inhibits the glucose-sensing receptor T1r3 expressed in mouse pancreatic B-cells. *J Endocrinol*. 2015;226:57-66.

29. Kyriazis GA, Smith KR, Tyrberg B, Hussain T, Pratley RE. Sweet taste receptors regulate basal insulin secretion and contribute to compensatory insulin hypersecretion during the development of diabetes in male mice. *Endocrinology*. 2014;155:2112-2121.

30. Oduori OS, Murao N, Shimomura K, et al. Gs/Gq signaling switch in β cells defines incretin effectiveness in diabetes. *J Clin Invest*. 2020;130(12):6639-6655. doi:10.1172/JCI140046

31. Hashim M, Yokoi N, Takahashi H, et al. Inhibition of SNAT5 induces incretin-responsive state from incretin-unresponsive state in pancreatic β-cells: study of β-cell spheroid clusters as a model. *Diabetes*. 2018;67(9):1795-1806. doi:10.2337/db17-1486

32. Kreuzberg K. Interaction of D-fructose and fructose 1-phosphate with yeast phosphofructokinase and its influence on glycolytic oscillations. *Biochim Biophys Acta Enzymol*. 1978;527:229-238.

33. Mapungwana SM, Davies DR. The effect of fructose on pyruvate kinase activity in isolated hepatocytes. Inhibition by allantoin and alanine. *Biochem J*. 1982;208:171-178.

34. Taylor SR, Ramsamooj S, Liang RJ, et al. Dietary fructose improves intestinal cell survival and nutrient absorption. *Nature*. 2021;597(7875):263-267. doi:10.1038/s41586-021-03827-2

35. Chandel NS. Glycolysis. *Cold Spring Harb Perspect Biol*. 2021;13:a040535.

36. Jiang J-k, Boxer MB, Vander Heiden MG, et al. Evaluation of thieno [3, 2-b] pyrrole [3, 2-d] pyridazinones as activators of the tumor cell specific M2 isoform of pyruvate kinase. *Bioorg Med Chem Lett*. 2010;20(11):3387-3393. doi:10.1016/j.bmcl.2010.04.015

37. Chandel, NS. Glycolysis. *Cold Spring Harbor Perspectives in Biology*. 2021;13(5):a040535. doi:10.1101/cshperspect.a040535

38. Abulizi A, Cardone RL, Stark R, et al. Multi-tissue acceleration of the mitochondrial phosphoenolpyruvate cycle improves whole-body metabolic health. *Cell Metab*. 2020;32:751-766. e11.

39. Abdelmalek MF, Lazo M, Horska A, et al. Higher dietary fructose is associated with impaired hepatic adenosine triphosphate homeostasis in obese individuals with type 2 diabetes. *Hepatology*. 2012;56(3):952-960. doi:10.1002/hep.25741

40. Colsoul B, Schraenen A, Lemaire K, et al. Loss of high-frequency glucose-induced Ca^{2+} oscillations in pancreatic islets correlates with impaired glucose tolerance in Trpm5−/− mice. *Proc Natl Acad Sci USA*. 2010;107:5208-5213.

41. Shigeto M, Ramracheya R, Tarasov AI, et al. GLP-1 stimulates insulin secretion by PKC-dependent TRPM4 and TRPM5 activation. *J Clin Invest*. 2015;125(12):4714-4728. doi:10.1172/JCI81975

42. Rorsman P, Ashcroft FM. Pancreatic β-cell electrical activity and insulin secretion: of mice and men. *Physiol Rev*. 2018;98:117-214.

43. Seino Y, Ogata H, Maekawa R, et al. Fructose induces glucose-dependent insulinotropic polypeptide, glucagon-like peptide-1 and insulin secretion: role of adenosine triphosphate-sensitive K+ channels. *J Diabetes Investig*. 2015;6(5):522-526. doi:10.1111/jdi.12356

44. Giroix M-H, Scruel O, Ladriere L, Sener A, Portha B, Malaisse WJ. Metabolic and secretory interactions between D-glucose and D-fructose in islets from GK rats. *Endocrinology*. 1999;140:5556-5565.

45. Sener A, Malaisse WJ. Hexose metabolism in pancreatic islets: metabolic and secretory responses to d-fructose. *Arch Biochem Biophys*. 1988;261(1):16-26. doi:10.1016/0003-9861(88)90099-9

46. Brown KS, Kalinowski SS, Megill JR, Durham SK, Mookhtiar KA. Glucokinase regulatory protein may interact with glucokinase in the hepatocyte nucleus. *Diabetes*. 1997;46:179-186.

47. McGuinness OP, Cherrington AD. Effects of fructose on hepatic glucose metabolism. *Curr Opin Clin Nutr Metab Care*. 2003;6:441-448.

48. Ashcroft SJ, Hedeskov CJ, Randle PJ. Glucose metabolism in mouse pancreatic islets. *Biochem J*. 1970;118:143-154.

49. Bartley C, Brun T, Oberhauser L, et al. Chronic fructose renders pancreatic β-cells hyper-responsive to glucose-stimulated insulin secretion through extracellular ATP signaling. *American Journal of Physiology-Endocrinology and Metabolism*. 2019;317:E25-E41.

50. Cirillo P, Gersch MS, Mu W, et al. Ketohexokinase-dependent metabolism of fructose induces proinflammatory mediators in proximal tubular cells. *J Am Soc Nephrol*. 2009;20:545-553.

51. Van Den Berghe G, Bronfman M, Vanneste R, Hers H. The mechanism of adenosine triphosphate depletion in the liver after a load of fructose. A kinetic study of liver adenylate deaminase. *Biochem J*. 1977;162:601-609.

52. Foster HR, Ho T, Potapenko E, et al. β-Cell deletion of the PKm1 and PKm2 isoforms of pyruvate kinase in mice reveals their essential role as nutrient sensors for the KATP channel. *elife*. 2022;11:e79422.

53. Lewandowski SL, Cardone RL, Foster HR, et al. Pyruvate kinase controls signal strength in the insulin secretory pathway. *Cell Metab*. 2020;32:736-750.e5.

54. Ho T, Potapenko E, Davis DB, Merrins MJ. A plasma membrane-associated glycolytic metabolon is functionally coupled to KATP channels in pancreatic α and β cells from humans and mice. *Cell Rep*. 2023;42(4):112394. doi:10.1016/j.celrep.2023.112394

55. Merrins MJ, Kibbey RG. Glucose regulation of β-cell KATP channels: it is time for a new model! *Diabetes*. 2024;73:856-863.

56. Corradi J, Thompson B, Fletcher PA, Bertram R, Sherman AS, Satin LS. KATP channel activity and slow oscillations in pancreatic beta cells are regulated by mitochondrial ATP production. *J Physiol*. 2023;601(24):5655-5667. doi:10.1113/JP284982

57. Rutter GA, Sweet IR. Glucose regulation of β-cell KATP channels: is a new model needed? *Diabetes*. 2024;73:849-855.

58. Satin LS, Corradi J, Sherman AS. Do we need a new hypothesis for KATP closure in β-cells? Distinguishing the baby from the bathwater. *Diabetes*. 2024;73:844-848.

59. Iizuka K. Recent progress on fructose metabolism—Chrebp, fructolysis, and polyol pathway. *Nutrients*. 2023;15:1778.

60. Patel C, Sugimoto K, Douard V, et al. Effect of dietary fructose on portal and systemic serum fructose levels in rats and in KHK−/− and GLUT5−/− mice. *Am J Physiol Gastrointest Liver Physiol*. 2015;309:G779-G790.

61. Sugimoto K, Hosotani T, Kawasaki T, et al. Eucalyptus leaf extract suppresses the postprandial elevation of portal, cardiac and peripheral fructose concentrations after sucrose ingestion in rats. *J Clin Biochem Nutr*. 2010;46(3):205-211. doi:10.3164/jcbn.09-93

SUPPORTING INFORMATION

Additional supporting information can be found online in the Supporting Information section at the end of this article.